Journal of Sound and Vibration (1999) **224**(4), 591–624
Article No. jsvi.1999.2193, available online at http://www.idealibrary.com on IDEAL®

NON-LINEAR VIBRATION OF BEAMS WITH INTERNAL RESONANCE BY THE HIERARCHICAL FINITE-ELEMENT METHOD

P. RIBEIRO

DEMEGI, Faculdade de Engenharia, Universidade do Porto, Rua dos Bragas, 4099 Porto Codex, Portugal

AND

M. PETYT

Institute of Sound and Vibration Research, University of Southampton, Southampton SO17 1BJ, England

(*Received* 26 *June* 1998, *and in final form* 14 *January* 1999)

The hierarchical finite-element (HFEM) and the harmonic balance methods (HBM) are used to investigate the geometrically non-linear free and steady-state forced vibrations of uniform, slender beams. The beam analogue of von Kármán's non-linear strain–displacement relationships are employed and the middle plane in-plane displacements are included in the model. The equations of motion are developed by applying the principle of virtual work and are solved by a continuation method, 1 : 3 and 1 : 5 internal resonances are discovered and their consequences are discussed. The convergence properties of the HFEM are analyzed and it is demonstrated that the HFEM model requires far fewer degrees of freedom than the *h*-version of the FEM models presented in the literature.

1. INTRODUCTION

As the displacement amplitude of a beam with fixed ends increases, the stiffness increases due to the effect of the membrane forces. Therefore, the non-linear normal mode [1] is, in general, amplitude dependent [2, 3] and the resonance frequency changes with the vibration amplitude. Consequently, the natural frequencies may become commensurable and conditions may exist for strong interaction of the modes involved. As a result energy is interchanged between those modes and the response is multi-modal. This phenomena is known as internal resonance [4, 5].

Nayfeh and Balachandran [6] reviewed theoretical and experimental studies on the influence of modal interactions on the non-linear response of harmonically excited structural systems. The authors concluded that different experiments have shown the existence of internal resonances and that these are responsible for "interesting, unusual and dangerous phenomena", as, for example, the instability of the planar motions of a symmetric beam resulting from a harmonic planar force.

0022-460X/99/290591 + 34 $30.00/0

The finite-element method (FEM) is based on approximating the solution of a problem by means of admissible functions. The *h*-version of the finite-element method, in which better approximations are achieved by refining the mesh, and the harmonic balance method have been applied to study the effect of internal resonances in the non-linear vibration of beams. In reference [7] the response curve due to a harmonic excitation was constructed using the Newton method and the phase angle as a parameter. A 1:3 internal resonance was detected in a clamped-hinged beam and resulted in looping characteristics of the response curve. Lewandowski [8–10] applied the Newton method and used the arc-length as a parameter, to describe the backbone curves (amplitude of vibration – resonance frequency relations) of simply supported, hinged-clamped and two-span beams, and the frequency response function (FRF) curves of simply supported, one- and two-span beams. 1:3 internal resonances were found and resulted in secondary branches or in an increase of the curvature of the backbone curves and FRF curves.

Generally, the solution of the non-linear equations of motion can only be obtained approximately and iteratively, with a reconstruction of the model in each iteration. The superposition principle is not applicable in non-linear problems and multiple solutions can exist. Consequently, a non-linear dynamic analysis is much more complicated than a linear one and the time needed to obtain the solution increases considerably with the number of degrees of freedom (d.o.f.). This number tends to become particularly high if, as is the case in the presence of internal resonances, high-order modes and different frequencies are involved in the response of the structure. Hence, an accurate model with a reduced number of degrees of freedom is very beneficial.

In the *p*-version of the FEM, the accuracy of the approximation is improved by increasing the number of shape functions over the elements, keeping the mesh constant. If the set of functions, corresponding to an approximation of lower order p, constitutes a subset of the set of functions corresponding to the approximation of order $p + 1$, then the *p*-version of the FEM is called the "hierarchical finite element method" (HFEM). The HFEM has, amongst others, the following advantages over the *h*-version of the FEM:

(i) the HFEM's linear matrices possess the embedding property [11] and the non-linear matrices of an approximation of lower order can be used in the derivation of the non-linear matrices of the improved approximation.

(ii) Simple structures can be modelled using just one element, or "super-element", thus there are no inter-element continuity requirements and the assemblage of the elements is avoided.

(iii) The HFEM tends to give accurate results with fewer d.o.f. than the *h*-version of the FEM [11–18]. This is particularly true for smooth solutions, since fine mesh generation is advantageous in the vicinity of singular points [19].

As a consequence of these properties, the HFEM model of a structure potentially requires less time to be produced and to be solved than an *h*-version of the FEM's model.

In this paper, a HFEM model of isotropic beams is presented and the free and steady-state forced vibrations of simply supported (ss) and clamped–clamped (cc) beams are studied. Results are compared with other published ones and it is

demonstrated that the HFEM model requires far fewer d.o.f. than the *h*-version of the FEM models. 1 : 3 and 1 : 5 internal resonances are found and the variation of the non-linear mode shape during the period of vibration and with the amplitude of vibration is shown.

2. BEAM EQUATIONS OF MOTION

A beam, its local and global co-ordinate systems are shown in Figure 1. ξ is a non-dimensional element, or local, co-ordinate; x, y and z are global co-ordinates. The full beam is going to be modelled with only one element, therefore, the relation between ξ and x is given by

$$\xi = \frac{2x}{L}. \tag{1}$$

The beam is assumed to be elastic and isotropic, with small uniform thickness h. The effects of transverse shear deformations and rotatory inertia are neglected. The transverse deflection, w, is large compared with the beam thickness — leading to geometrical non-linearity — but is very small compared with the length, L, of the beam ($w \ll L$). With these conditions the beam analogue of von Kármán's plate theory [20] can be applied. The in-plane displacement, u, and the transverse displacement w, at a point of the beam are hence given by

$$u(x, z, t) = u^0(x, t) - zw^0_{,x},$$

$$w(x, z, t) = w^0(x, t), \tag{2}$$

in which u^0 and w^0 are the values of the displacement components u and w at the middle plane: "$_{,x}$" denotes the derivative with respect to x. For convenience of notation, the superscript 0 will be omitted in u^0 and w^0. Henceforth, u and w stand for the middle plane displacements.

The strain–displacement relationship may be expressed in the form

$$\varepsilon_x = \varepsilon_x^0 + z\kappa_x, \tag{3}$$

where ε_x^0 is the non-linear in-plane strain at the middle plane of the beam, defined by

$$\varepsilon_x^0 = u_{,x} + \tfrac{1}{2}(w_{,x})^2. \tag{4}$$

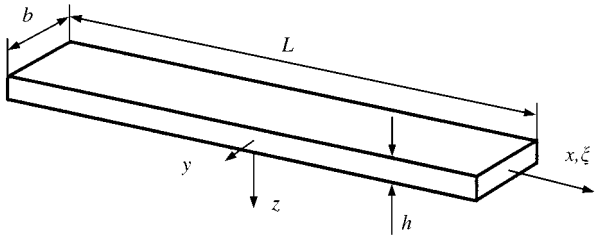

Figure 1. Beam, local and global co-ordinate systems

and κ_x is the beam curvature given by

$$\kappa_x = -w_{,xx} \tag{5}$$

The vector $\{\mathbf{d}\}$, formed by the displacement components u and w, may be expressed as the combination of the hierarchical shape functions:

$$\{\mathbf{d}\} = \begin{Bmatrix} u \\ w \end{Bmatrix} = [\mathbf{N}]\{\mathbf{q}\}, \tag{6}$$

$$[\mathbf{N}] = \begin{bmatrix} g_1 g_2 \dots g_{p_i} & 0 \\ 0 & f_1 f_2 \dots f_{p_o} \end{bmatrix} = \begin{bmatrix} \lfloor \mathbf{N}^u \rfloor & 0 \\ 0 & \lfloor \mathbf{N}^w \rfloor \end{bmatrix}, \tag{7}$$

$$\lfloor \mathbf{N}^u \rfloor = \lfloor g_1(x) \quad g_2(x) \quad \cdots \quad g_{p_i}(x) \rfloor, \tag{8}$$

$$\lfloor \mathbf{N}^w \rfloor = \lfloor f_1(x) \quad f_2(x) \quad \cdots \quad f_{p_o}(x) \rfloor, \tag{9}$$

$$\{\mathbf{q}\}^{\mathrm{T}} = \lfloor \{\mathbf{q}_u\}^{\mathrm{T}} \{\mathbf{q}_w\}^{\mathrm{T}} \rfloor = \lfloor q_u(1) \quad q_u(2) \quad \dots \quad q_u(p_i) \quad q_w(1) \quad q_w(2) \quad \dots \quad q_w(p_o) \rfloor, \tag{10}$$

where $[\mathbf{N}]$ is the matrix of shape functions, $\lfloor \mathbf{N}^u \rfloor$ and $\lfloor \mathbf{N}^w \rfloor$ are, respectively, the in-plane and the out-of-plane shape function vectors, $\{\mathbf{q}\}$ is the vector of generalized nodal displacements, $\{\mathbf{q}_u\}$ and $\{\mathbf{q}_w\}$ are respectively the generalized displacement vectors in the x and z directions, p_i is the number of in-plane shape functions and p_o is the number of out-of-plane shape functions. Only the shape functions that satisfy the geometric boundary conditions are included in the model. The set of shape functions used is derived from Rodrigues' form of Legendre polynomials [12, 13] and are shown in Appendix A. The in-plane shape functions are given by

$$g_{r-2} = \sum_{n=0}^{INT(r/2)} \frac{(-1)^n (2r-2n-5)!!}{2^n n!(r-2n-1)!} \xi^{r-2n-1}, \quad r > 2 \tag{11}$$

and the out-of-plane shape functions are given by

$$f_{r-2} = \sum_{n=0}^{\mathrm{INT}(r/2)} \frac{(-1)^n (2r-2n-7)!!}{2^n n!(r-2n-1)!} \xi^{r-2n-1}, \quad r > 4, \tag{12}$$

where $r!! = r(r-2)\dots(2 \text{ or } 1)$, $0!! = (-1)!! = 1$ and $\mathrm{INT}(r/2)$ denotes the integer part of $r/2$. These shape functions satisfy fully clamped boundary conditions. To analyze beams with different boundary conditions, other shape functions — for example third-order polynomials — are added to the model.

The strain (3) can be expressed as

$$\varepsilon_x = \lfloor 1 \quad z \rfloor \{\boldsymbol{\varepsilon}\}, \tag{13}$$

where

$$\{\boldsymbol{\varepsilon}\} = \begin{Bmatrix} u_{,x} \\ -w_{,xx} \end{Bmatrix} + \begin{Bmatrix} w_{,x}^2/2 \\ 0 \end{Bmatrix} = \begin{Bmatrix} \varepsilon_0^p \\ \varepsilon_0^b \end{Bmatrix} + \begin{Bmatrix} \varepsilon_L^p \\ 0 \end{Bmatrix} = \{\boldsymbol{\varepsilon}_1\} + \{\boldsymbol{\varepsilon}_2\}. \tag{14}$$

In equation (14), the strain is divided into linear, $\{\boldsymbol{\varepsilon}_1\}$, and geometrically non-linear, $\{\boldsymbol{\varepsilon}_2\}$ or $\boldsymbol{\varepsilon}_L^p$, strains. The linear strain $\{\boldsymbol{\varepsilon}_1\}$, is subdivided into the linear membrane $\boldsymbol{\varepsilon}_0^p$, and bending, $\boldsymbol{\varepsilon}_0^b$, strains. With this approach, common in plates [21], the stiffness matrix is clearly divided into parts related to the different strains.

Using equation (6), $\boldsymbol{\varepsilon}_0^p$ and $\boldsymbol{\varepsilon}_0^b$ may be expressed as

$$\boldsymbol{\varepsilon}_0^p = \lfloor \mathbf{N}_{,x}^u \rfloor \{\mathbf{q}_u\}, \tag{15}$$

$$\boldsymbol{\varepsilon}_0^b = -\lfloor \mathbf{N}_{,xx}^w \rfloor \{\mathbf{q}_w\}. \tag{16}$$

The geometrically non-linear membrane strain, $\boldsymbol{\varepsilon}_L^p$, is defined as

$$\boldsymbol{\varepsilon}_L^p = \tfrac{1}{2}(w_{,x})^2 \tag{17}$$

and may be expressed in the form

$$\boldsymbol{\varepsilon}_L^p = \tfrac{1}{2}\{\mathbf{q}_w\}^{\mathrm{T}} \lfloor \mathbf{N}_{,x}^w \rfloor^{\mathrm{T}} \lfloor \mathbf{N}_{,x}^w \rfloor \{\mathbf{q}_w\}. \tag{18}$$

The constitutive equation of an isotropic beam is

$$\sigma_x = E\varepsilon_x, \tag{19}$$

where E is Young's modulus.

The stress and moment resultants (per unit width) are defined by

$$T_x = \int_z \sigma_x \, \mathrm{d}z, \tag{20}$$

$$M_x = \int_z \sigma_x z \, \mathrm{d}z. \tag{21}$$

Substituting equations (13) and (19) into equations (20, 21) results in

$$\begin{Bmatrix} T \\ M \end{Bmatrix} = \begin{bmatrix} A & B \\ B & D \end{bmatrix} \{\boldsymbol{\varepsilon}\} = [\mathbf{E}]\{\boldsymbol{\varepsilon}\}, \tag{22}$$

where $[\mathbf{E}]$ is the elastic matrix; A, B and D are the extension, coupling and bending coefficients given by

$$A, B, D = \int_z (1, z, z^2) E \, \mathrm{d}z. \tag{23}$$

For isotropic beams, A, B and D are the following scalar quantities:

$$A = Eh, \quad B = 0, \quad D = Eh^3/12 = EI/b, \tag{24}$$

I is the second moment of area of the cross-section of the beam and $B = 0$ reflects the absence of coupling between extension and bending.

For undamped systems, the principle of virtual work states that

$$\delta W_{in} + \delta W_V + \delta W_{ex} = 0, \tag{25}$$

where δW_{in}, δW_V and δW_{ex} are respectively the work done by the inertia, internal and external forces due to a virtual displacement $\{\delta \mathbf{d}\}$, which is given by

$$\{\delta \mathbf{d}\} = \begin{Bmatrix} \delta u \\ \delta w \end{Bmatrix} = [\mathbf{N}]\{\delta \mathbf{q}\}. \tag{26}$$

Making use of D'Alembert's principle, the following expression for the virtual work of the inertia forces results:

$$\delta W_{in} = -\rho hb \int_L \{\delta \mathbf{d}\}^{\mathrm{T}} \{\ddot{\mathbf{d}}\} \, \mathrm{d}L = -\{\delta \mathbf{q}\}^{\mathrm{T}} [\mathbf{M}] \{\ddot{\mathbf{q}}\}, \tag{27}$$

$$[\mathbf{M}] = \rho hb \int_L [\mathbf{N}]^{\mathrm{T}} [\mathbf{N}] \, \mathrm{d}L, \tag{28}$$

where ρ is the mass per unit volume of the material that constitutes the beam, b is the width of the beam, $[\mathbf{M}]$ represents the mass matrix and $\{\ddot{\mathbf{q}}\} = \mathrm{d}^2\{\mathbf{q}\}/\mathrm{d}t^2$.

The variation δW_V may be expressed as

$$\delta W_V = -b \int_L (\{\delta \boldsymbol{\varepsilon}_1\}^{\mathrm{T}} + \{\delta \boldsymbol{\varepsilon}_2\}^{\mathrm{T}})[\mathbf{E}](\{\boldsymbol{\varepsilon}_1\} + \{\boldsymbol{\varepsilon}_2\}) \, \mathrm{d}L. \tag{29}$$

The linear stiffness matrix $[\mathrm{K}_1]$ and the non-linear stiffness matrices $[\mathbf{K}_2]$, $[\mathbf{K}_3]$ and $[\mathbf{K}_4]$ are defined by

$$b \int_L \{\delta \boldsymbol{\varepsilon}_1\}^{\mathrm{T}} [\mathbf{E}] \{\boldsymbol{\varepsilon}_1\} \, \mathrm{d}L = \{\delta \mathbf{q}\}^{\mathrm{T}} [\mathbf{K}_1] \{\mathbf{q}\}, \tag{30}$$

$$b \int_L \{\delta \boldsymbol{\varepsilon}_1\}^{\mathrm{T}} [\mathbf{E}] \{\boldsymbol{\varepsilon}_2\} \, \mathrm{d}L = \{\delta \mathbf{q}\}^{\mathrm{T}} [\mathbf{K}_2] \{\mathbf{q}\}, \tag{31}$$

$$b \int_L \{\delta \boldsymbol{\varepsilon}_2\}^{\mathrm{T}} [\mathbf{E}] \{\boldsymbol{\varepsilon}_1\} \, \mathrm{d}L = \{\delta \mathbf{q}\}^{\mathrm{T}} [\mathbf{K}_3] \{\mathbf{q}\}, \tag{32}$$

$$b \int_L \{\delta \boldsymbol{\varepsilon}_2\}^{\mathrm{T}} [\mathbf{E}] \{\boldsymbol{\varepsilon}_2\} \, \mathrm{d}L = \{\delta \mathbf{q}\}^{\mathrm{T}} [\mathbf{K}_4] \{\mathbf{q}\}; \tag{33}$$

$[\mathbf{K}_3]$ and $[\mathbf{K}_2]$ are related by $[\mathbf{K}_3] = 2[\mathbf{K}_2]^{\mathrm{T}}$ [13]. Using equations (30)–(33), equation (29) is rewritten as

$$\delta W_V = -\{\delta\mathbf{q}\}^{\mathrm{T}}([\mathbf{K}_1] + [\mathbf{K}_2] + [\mathbf{K}_3] + [\mathbf{K}_4])\{\mathbf{q}\}. \tag{34}$$

If $\bar{P}_j(t)$ represents a concentrated force acting at the point $x = x_j$ and $\bar{P}_d(x, t)$ represents a distributed force, the virtual work of the external forces is given by

$$\delta W_{ex} = \int_L [\bar{P}_j(t)\,\delta(x - x_j) + \bar{P}_d(x, t)]\,\delta w(x, t)\,\mathrm{d}L = \{\delta\mathbf{q}_w\}^{\mathrm{T}}\{\bar{\mathbf{P}}(t)\}, \tag{35}$$

where $\{\bar{\mathbf{P}}(t)\}$ represents the vector of generalized external applied forces and $\delta(x - x_j)$ represents a spatial Dirac delta function given by

$$\delta(x - x_j) = 0, \quad x \neq x_j,$$

$$\int_0^L \delta(x - x_j)\,\mathrm{d}x = 1 \tag{36}$$

so that $\bar{P}_j(t)\delta(x - x_j)$ has units of distributed force (N/m).

Mass proportional hysteretic damping is used. This depends on the damping factor β, which is given by

$$\beta = \omega_{\ell 1}^2 \times \alpha, \tag{37}$$

where $\omega_{\ell 1}$ represents the fundamental linear frequency and α the loss factor [22].

The mass matrix $[\mathbf{M}]$ is formed by $[\mathbf{M}_p]$ and $[\mathbf{M}_b]$, which are the in-plane and bending mass matrices. The linear stiffness matrix $[\mathbf{K}_1]$ is formed by the in-plane, $[\mathbf{K}_{1p}]$, and bending, $[\mathbf{K}_{1b}]$, linear stiffness matrices. The in-plane inertia can be neglected for slender beams [23] and $\{\mathbf{q}_u\}$ is eliminated. The damping contribution due to the axial stress is also negligible compared to that due to the bending stress [24]. The equations of motion are thus of the following form:

$$[\mathbf{M}_b]\{\ddot{\mathbf{q}}_w\} + \frac{\beta}{\omega}[\mathbf{M}_b]\{\dot{\mathbf{q}}_w\} + [\mathbf{K}_{1b}]\{\mathbf{q}_w\} + [\mathbf{K}nl]\{\mathbf{q}_w\} = \{\bar{\mathbf{P}}\}, \tag{38}$$

$$[\mathbf{K}nl] = [\mathbf{K}_4] - 2[\mathbf{K}_2]^{\mathrm{T}}[\mathbf{K}_{1p}]^{-1}[\mathbf{K}_2]. \tag{39}$$

The non-linear stiffness matrix $[\mathbf{K}nl]$ is a quadratic function of the generalized transverse displacements, $\{\mathbf{q}_w\}$. $[\mathbf{K}_2]$ and $[\mathbf{K}_4]$ represent the non-zero part of the respective non-linear stiffness matrices defined in equations (31) and (33).

Only harmonic excitations of the form $\{\bar{\mathbf{P}}\} = \{\mathbf{P}\}\cos(\omega t)$ will be applied and the steady-state response $\{\mathbf{q}_w(t)\}$ is expressed as

$$\{q_w(t) = \sum_{i=1,3}^{2k-1} \{w_{ci}\}\cos(i\omega t) + \{w_{si}\}\sin(i\omega t), \tag{40}$$

where k is an integer that represents the number of harmonics used.

This equation is inserted into the equations of motion (38) and the HBM is employed [4]. This method, in which the coefficients of the same harmonic components are compared, can be easily implemented in a program produced with the symbolic manipulator *Maple* [18, 25]. The resulting equations of motion in the frequency domain are of the form

$$\{\mathbf{F}\} = (-\omega^2[\mathbf{M}] + [\mathbf{C}] + [\mathbf{KL}] + [\mathbf{KNL}(\{\mathbf{w}\})])\{\mathbf{w}\} - \{\mathbf{P}\} = \{\mathbf{0}\}, \qquad (41)$$

where $[\mathbf{M}]$ represents the mass matrix, which is a function of $[\mathbf{M}_b]$, $[\mathbf{C}]$ the damping matrix, which is a function of $\beta[\mathbf{M}_b]$, $[\mathbf{KL}]$ the linear stiffness matrix, function of $[\mathbf{K}_{1b}]$, and $[\mathbf{KNL}(\{\mathbf{w}\})]$ the non-linear stiffness matrix, which is a function of $[\mathbf{K}_2]$ and $[\mathbf{K}_4]$ and depends quadratically on the generalized displacements $\{\mathbf{w}\}^{\mathrm{T}} = \lfloor w_{c1} \;\; w_{s1} \;\; w_{c3} \;\; w_{s3} \;\; \cdots \;\; w_{si} \rfloor$. The total number of d.o.f. of the HFEM model, n, is $n = 2kp_o$, with damping, and $n = kp_o$, without damping.

3. THE CONTINUATION METHOD

In forced vibration, the solutions of the equations of motion in the non-resonant region are calculated by Newton's method [21]. In free harmonic vibration, a simple iterative method based on a consecutive solution of an eigenvalue problem [13–15, 26, 27], named *linearized updated mode* (LUM) as in reference [26], is utilized.

However, in forced vibration and in the vicinity of resonance frequencies, multiple solutions exist and convergence is not always achieved with the Newton method alone. Also in multi-harmonic free vibration convergence is difficult with the LUM method [27]. Therefore, a continuation method is utilized in most of the analysis. This method is outlined in the following paragraphs, details are given in references [8–10, 18].

The continuation method is composed of two main loops. In the external loop a predictor to the solution is defined. The prediction of the vector of generalized co-ordinates is obtained by using the two last determined vectors of the curve, $\{\mathbf{w}\}_i$ and $\{\mathbf{w}\}_{i-1}$, as follows:

$$\{\mathbf{w}\}_{i+1} = \{\mathbf{w}\}_i + \Delta\{w\}_{i+1}, \quad \Delta\{\mathbf{w}\}_{i+1} = (\{\mathbf{w}\}_i - \{\mathbf{w}\}_{i-1})\frac{\mathrm{d}waux}{\Delta w}. \qquad (42)$$

d$waux$ is the amplitude of the first increment vector, $\Delta\{\mathbf{w}\}_{i+1}$, and Δw is the amplitude of the vector $(\{\mathbf{w}\}_i - \{\mathbf{w}\}_{i-1})$. A prediction for the square of the frequency of vibration, ω_{i+1}^2, is calculated using the equations

$$\omega_{i+1}^2 = \omega_i^2 + \Delta\omega_0^2, \qquad (43)$$

$$\Delta\omega_0^2 = \pm s/(\{\delta\mathbf{w}\}_1^{\mathrm{T}}\{\delta\mathbf{w}\}_1)^{1/2}. \qquad (44)$$

The sign in equation (44) is chosen following that of the previous increment, unless the determinant, $|J|$, of the Jacobian of $\{F\}$, $[J]$, has changed sign. In the last case

a sign reversal is applied. s is the arc-length and $\{\delta\mathbf{w}\}_1$ is defined by the following equation [18]:

$$[\mathbf{J}]\{\delta\mathbf{w}\}_1 = [\mathbf{M}]\{\mathbf{w}\}_{i+1}. \tag{45}$$

The approximated solution is corrected in an internal loop. The corrections $\{\delta\mathbf{w}\}$ and $\delta\omega^2$ are obtained by applying Newton's method to equation (41):

$$[\mathbf{J}]\{\delta\mathbf{w}\} - [\mathbf{M}]\{\mathbf{w}\}_{i+1}\,\delta\omega^2 = -\{\mathbf{F}\}. \tag{46}$$

Variations in the frequency were considered in (46) and, consequently, one more equation is needed. This is obtained by constraining the distance between the two successive points of the frequency response function (FRF) curve, the arc-length s, to a fixed value:

$$s^2 = \|\Delta\{\mathbf{w}\}_{i+1}\|^2. \tag{47}$$

The iterations in the internal loop are repeated until the inequalities

$$|\delta\omega^2/\omega_{i+1}^2| < error1, \tag{48}$$

$$\|\{\delta\mathbf{w}\}\|\,\|\{\mathbf{w}\}_{i+1}\| < error2, \tag{49}$$

$$\|\{\mathbf{F}\}\| < error3, \tag{50}$$

are satisfied.

4. APPLICATIONS

4.1. BEAM PROPERTIES

The HFEM model will be applied to a cc and to a ss beam with the following geometric and material (aluminium DTDSO 70) properties: $h = 2$ mm, $b = 20$ mm, $L = 580$ mm, $I = (1/12)bh^3 = 1{\cdot}333(3) \times 10^{-11}\,\mathrm{m}^4$, $r = \sqrt{I/\Omega} = 5{\cdot}7735 \times 10^{-4}$ m, $E = 7 \times 10^{10}\,\mathrm{N/m}^2$, $\rho = 2778\,\mathrm{kg/m}^3$, where r represents the radius of gyration and Ω the area of the beam's cross-section.

4.2. FREE VIBRATION

4.2.1. Clamped–clamped beam

The linear modes of a beam clamped at both ends are symmetric or antisymmetric. In the harmonic solution, these symmetries are used to reduce the number of d.o.f. of the model. There is no difference between the first four linear natural frequencies obtained with $p_o = 5$ and the analytical ones [28] (Table 1). With five out-of-plane shape functions, $p_o = 5$, and five in-plane shape functions, $p_i = 5$, convergence of the non-linear harmonic solution is achieved (Table 2; w_m

TABLE 1
Natural linear frequencies cc beam (rad/s)

Mode	1	2	3	4
Exact [28]*	192·8	531·3	1041·6	1722
HFEM	192·8	531·3	1041·6	1722

*The data in reference [28] is provided with four significant digits

TABLE 2
Non-dimensional ($\omega/\omega_{\ell 1}$) first natural frequency

w_m/h	1·75	2
$p_o = p_i = 5$	1·6117	1·7530
$p_o = p_i = 7$	1·6117	1·7530

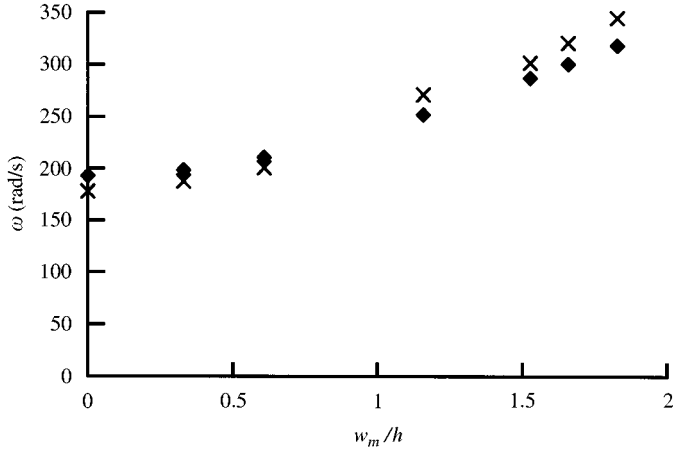

Figure 2. First resonance frequency of cc beam: ◆ HFEM; × experimental.

represents the maximum amplitude of vibration) and the harmonic HFEM's results are close to experimental ones [29] (Figure 2). Consequently, five out-of-plane and five in-plane shape functions were used in the harmonic model.

In the two and three harmonic solutions, in order to detect possible couplings between modes of different types of symmetry, symmetric and antisymmetric shape functions ($p_o = 7$ and $p_i = 10$) were used in the HFEM model.

The relations between the first linear frequencies and the fundamental linear frequency are $\omega_{\ell 2}/\omega_{\ell 1} = 2{\cdot}756$ and $\omega_{\ell 3}/\omega_{\ell 1} = 5{\cdot}404$. When the beam is vibrating in its first non-linear mode shape the hardening spring effect influences mainly the fundamental non-linear frequency.* Thus, the second frequency is never equal to

*This has been verified in all applications and in the literature. However, it was not proved.

TABLE 3
Natural frequencies ($\omega/\omega_{\ell 1}$) of cc beam

w_m/h*	0·5	1·0	1·5	2·0	2·25
One harmonic	1·0651	1·2377	1·4771	1·7530	1·8994
Two harmonics	1·0649	1·2351	1·4699	1·7453	1·9280
Three harmonics	1·0648	1·2370	1·4754	1·7631	1·9227
w_m/h*	2·50	2·75	3·00	3·25	—
One harmonic	2·0481	2·2021	2·3570	2·5137	
Two harmonics	2·0957	2·2919	2·5926	2·8946	—
Three harmonics	2·1052	2·3204	2·6122	2·9791	—

*For two and three harmonics the value of w_m/h is approximated (error $< 0{\cdot}6\%$ and $< 0{\cdot}16\%$, respectively).

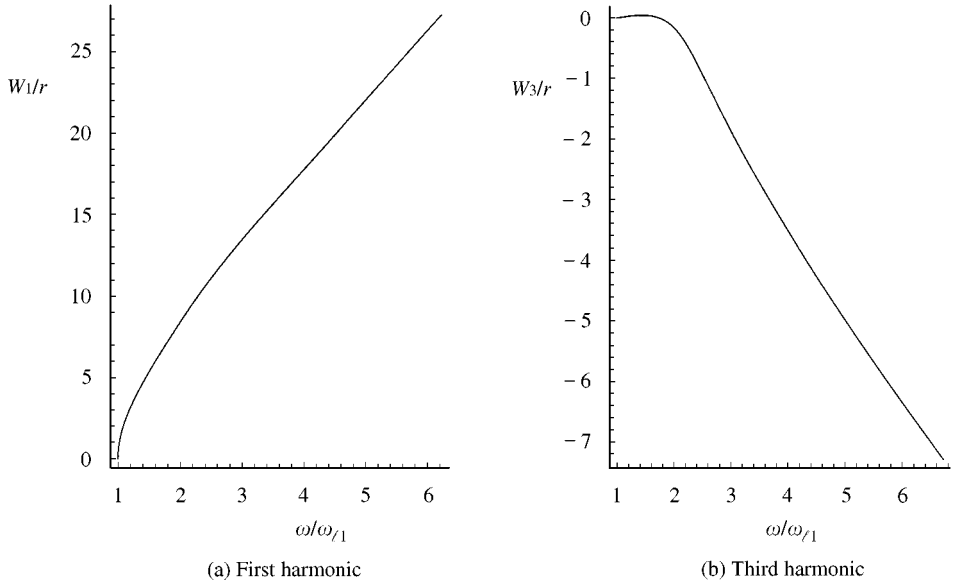

Figure 3. Backbone curves of cc beam. Amplitudes W_1 and W_3 calculated at $x = 0$.

three or five times the first one. It can be equal to twice $\omega_{\ell 1}$, but a system represented by the equations of motion (41), with $\{\bar{\mathbf{P}}\}$ equal to zero or harmonic with mean value zero, does not admit an excitation of the second harmonic [4, 30], because only odd harmonics are present in the frequency spectrum of the vibration. However, the third resonance frequency can be equal to three and five times the first one. Therefore, internal resonances of order 1 : 3 and 1 : 5 due to coupling between modes 1 and 3, are possible.

Table 3 compares the first resonance frequency obtained with one, two (the first and the third) and three (the first, the third and the fifth) harmonics, for different

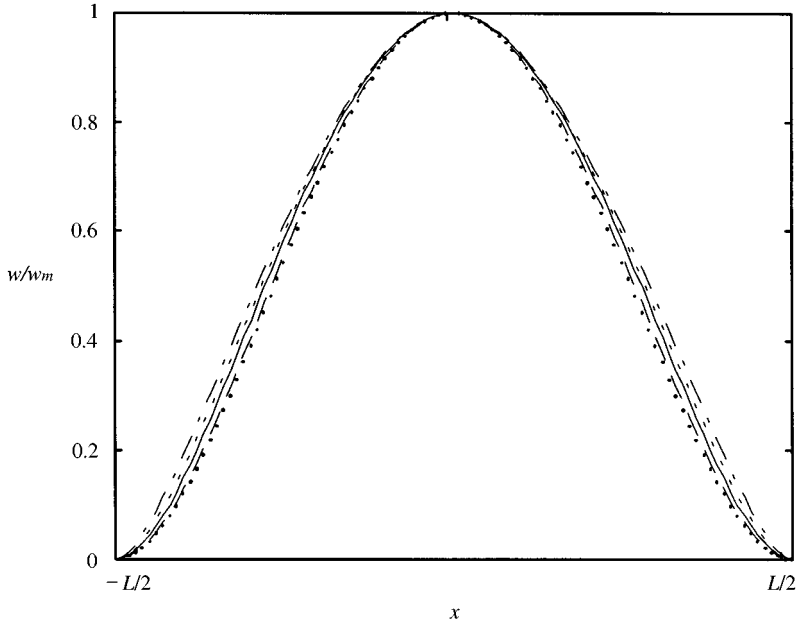

Figure 4. Mode shapes of the first harmonic of cc beam. ... linear mode, —— $\omega/\omega_{\ell 1} = 1{\cdot}2351$, —$\omega/\omega_{\ell 1} = 1{\cdot}7453$, – – $\omega/\omega_{\ell 1} = 2{\cdot}5926$, —– $\omega/\omega_{\ell 1} = 3{\cdot}8709$.

amplitudes, w_m, at the point $x = 0$. With the continuation method, because the arc-length is a parameter instead of the amplitude of vibration, the values of w_m/h are approximated. After $w_m/h = 2$, the results obtained with one harmonic are increasingly inaccurate. For the amplitudes studied the two harmonics approximation is accurate.

Figures 3(a) and 3(b) represent the backbone curves calculated with two harmonics. W_1 and W_3 are the amplitudes of the first and third harmonics respectively. In Figures 4 and 5 the mode shapes associated with different maximum amplitudes of vibration displacement are shown. The third harmonic has a growing role in the vibration of the beam, Figure 3(b), and is increasingly more affected by the third mode of vibration than by the first (Figure 5). Figure 6 — which was computed at $t = 2\pi mT$, where m is an integer and T represents the period of vibration — demonstrates that the shape assumed by the beam is significantly affected by the third harmonic. This is particularly true after $\omega/\omega_{\ell 1} \cong 1{\cdot}8$ ($\omega = 347{\cdot}83$ rad/s, $w_m/h = 2{\cdot}0264$).

If the first harmonic vibrates at $\omega = 347{\cdot}83$ rad/s then the third one will have a frequency of 1043·5 rad/s, which is very near to the third linear natural frequency (Table 1). Therefore, a 1 : 3 internal resonance occurs, the first mode couples with the third and as a result the importance of the third harmonic increases. Due to the mode coupling, the shape of the beam changes significantly during the period of vibration. An example of this variation can be seen in Figure 7, where the shape assumed by the beam is plotted at different instants along half a period of vibration.

The backbone curves represented in Figures 8–10 were calculated with three harmonics. W_1, W_3 and W_5 represent respectively the amplitudes of the first, third

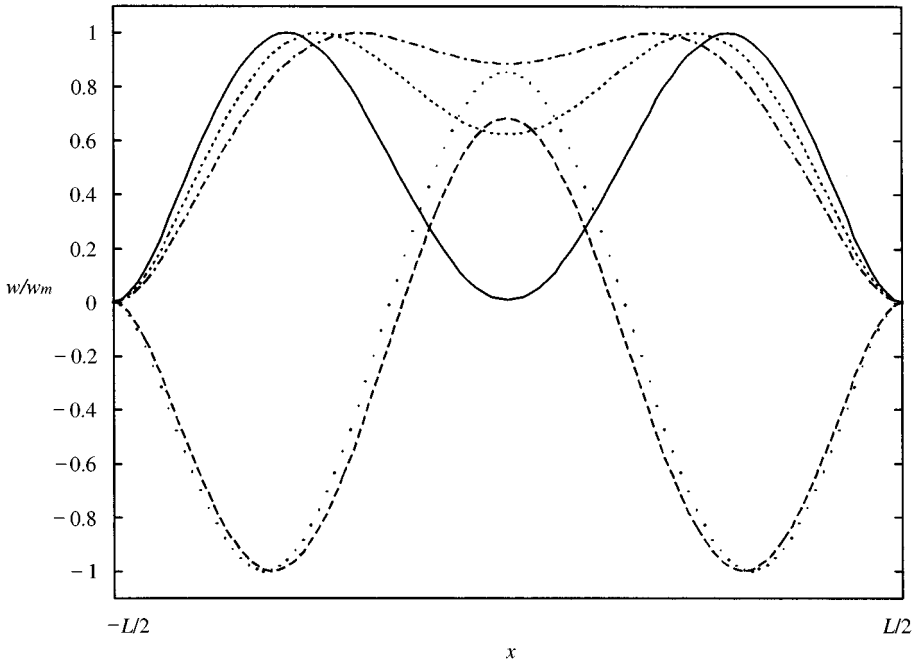

Figure 5. Mode shapes of the third harmonic of the cc beam. — – $W_1/h \ll 1$, $\omega/\omega_{\ell 1} \cong 1$, – – $\omega/\omega_{\ell 1} = 1{\cdot}2351$, —$\omega/\omega_{\ell 1} = 1{\cdot}7453$, —— $\omega/\omega_{\ell 1} = 2{\cdot}5926$, ··· $\omega/\omega_{\ell 1} = 3{\cdot}8709$.

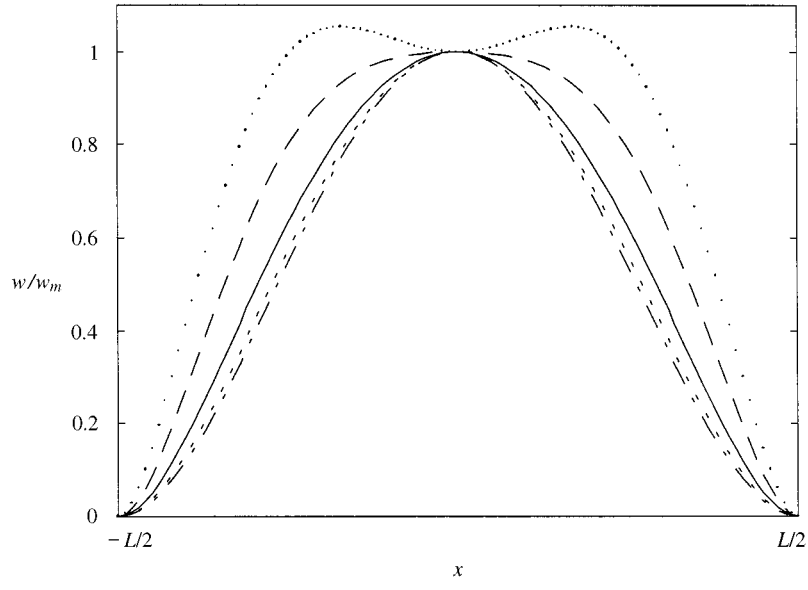

Figure 6. Shape of cc beam at $t = 2\pi mT$: -· $\omega/\omega_{\ell 1} = 1{\cdot}0001$, – – $\omega/\omega_{\ell 1} = 1{\cdot}2351$, —$\omega/\omega_{\ell 1} = 1{\cdot}7453$, —— $\omega/\omega_{\ell 1} = 2{\cdot}5926$, —– $\omega/\omega_{\ell 1} = 3{\cdot}8709$.

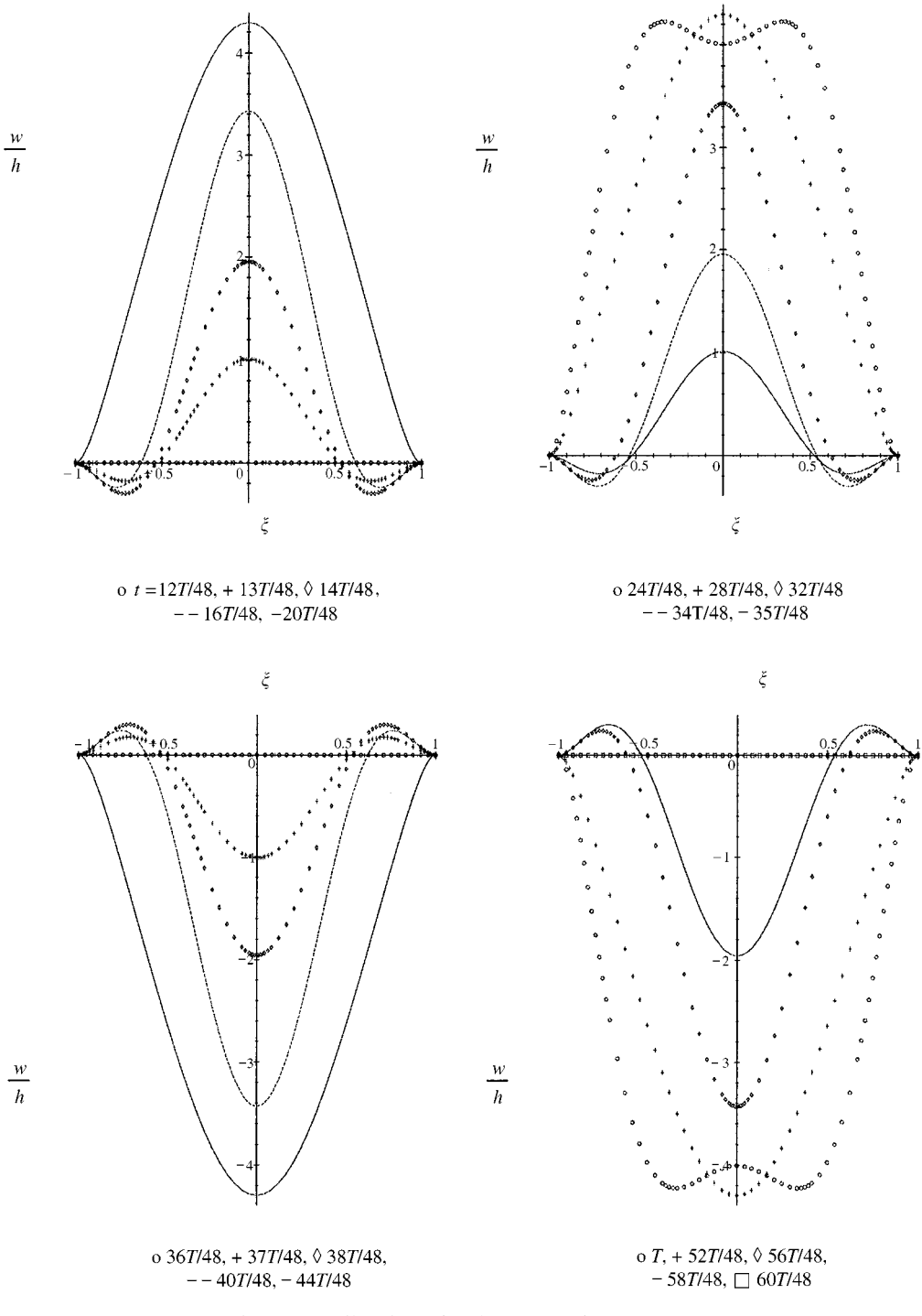

Figure 7. Vibration of cc beam at $\omega/\omega_{\ell 1} = 3{\cdot}84$.

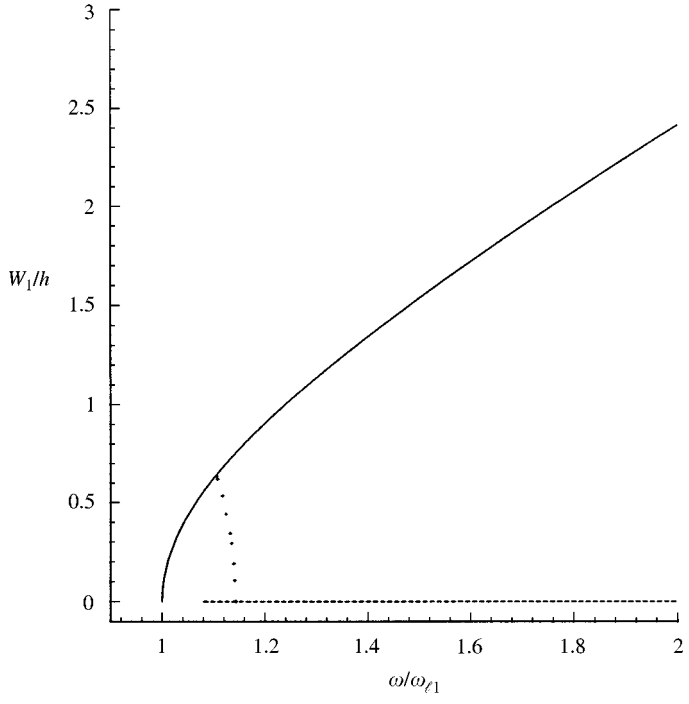

Figure 8. Backbone curve of cc beam defined by W_1/h and $\omega/\omega_{\ell 1}$. —— first main branch, + + + secondary branch, ····· second main branch.

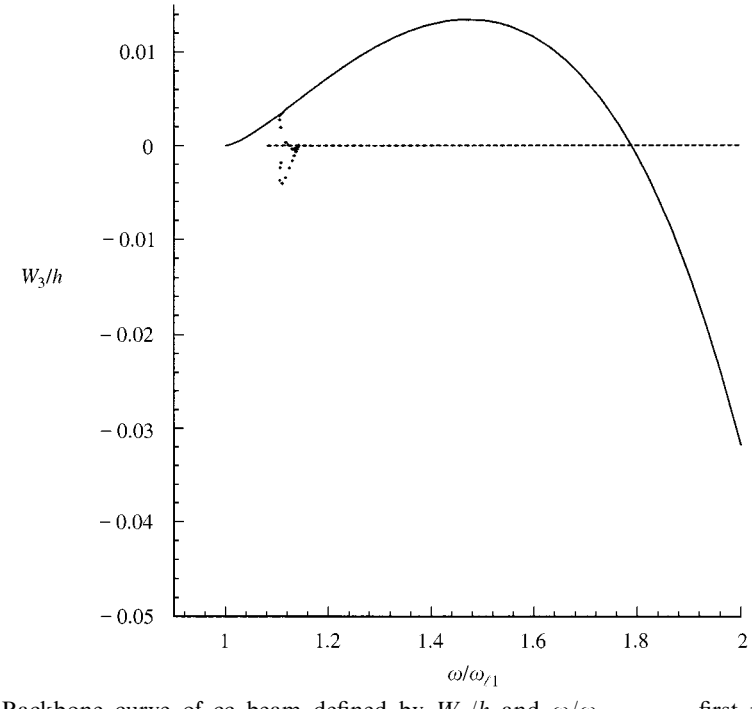

Figure 9. Backbone curve of cc beam defined by W_3/h and $\omega/\omega_{\ell 1}$. — — first main branch, + + + secondary branch, ····· second main branch.

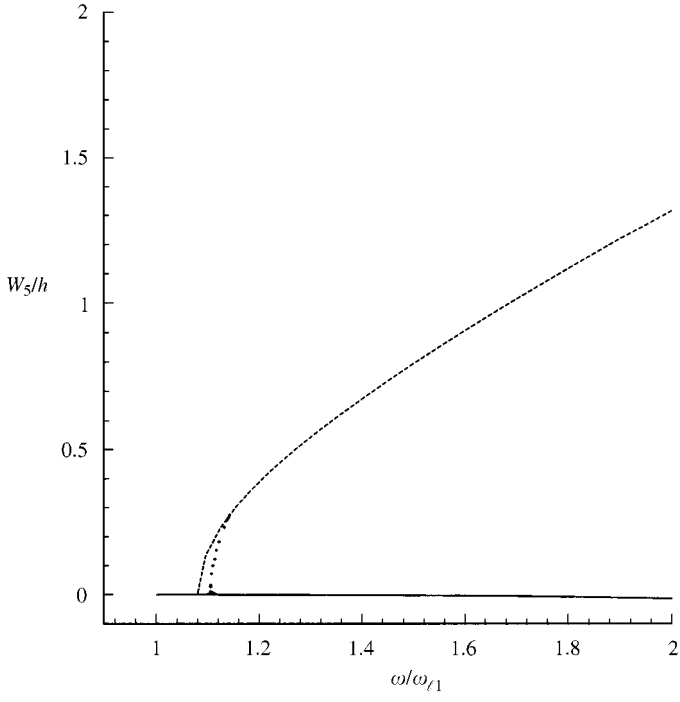

Figure 10. Backbone curve of beam defined by W_5/h and $\omega/\omega_{\ell 1}$. — first main branch, + + + secondary branch, ····· second main branch.

and fifth harmonics calculated at $x = 0{\cdot}25 \times L$. A modal coupling between the first and the third modes, due to a 1 : 5 internal resonance, was found. It resulted in a bifurcation point and in a secondary branch that links the first main branch with the second main branch. A bifurcation point exists as well in this last branch. The determinant of the matrix $[\mathbf{J}]$ changed sign between the two successive points of the main branches that enclose the respective bifurcation points.

The first main branch calculated with three harmonics is similar to the one calculated with two harmonics (and until $\omega/\omega_{\ell 1} \cong 2$, it is similar to the one calculated with only one harmonic, Table 3). The second main branch is, for the frequencies analyzed, related only to the third mode and to the fifth harmonic. The secondary branch is defined mainly by the first and fifth harmonics. In this branch, the first harmonic is related to the first mode, the fifth harmonic to the third mode and the third harmonic to both the first and fifth modes [Figures (11a–c)]. Both the secondary branch and the second main branch were overlooked by the two harmonics solution.

4.2.2. *Simply supported beam*

In this section, the free vibration of a ss beam is studied using two harmonics in expression (40), in order to, by comparison with published results, validate the HFEM model and show that it requires less d.o.f. than the *h*-version of the FEM.

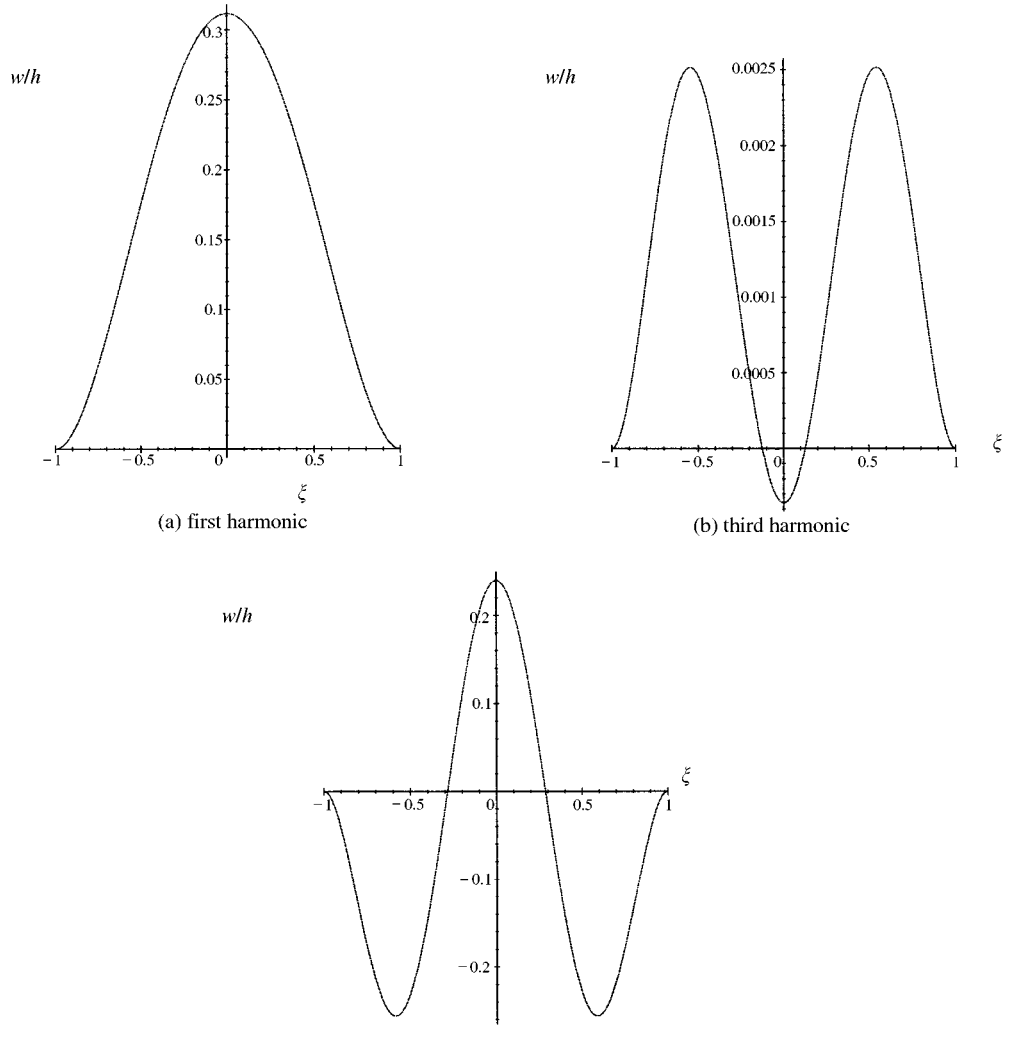

Figure 11. Mode shapes of cc beam at point $\omega/\omega_{\ell 1} = 1{\cdot}1339$ of secondary branch.

The relation between the first two linear frequencies of the ss beam is $\omega_{l2}/\omega_{\ell 1} = 4{\cdot}000$, and consequently modal coupling between the first (symmetric) and the second (antisymmetric) modes is possible. This means that both the symmetric and antisymmetric out-of-plane and in-plane shape functions should be used in the model. Moreover, comparing with the cc case, two additional shape functions had to be introduced — the shape functions f_1 and f_2 shown in Appendix A — so that the boundary conditions were satisfied.

In Table 4, the value of the fundamental linear frequency is compared with the values from the literature [8, 28, 31]. The value of λ calculated in reference [8] with 12 d.o.f. is larger — and therefore not so accurate (the HFEM linear solutions converge from above [11]) — than the HFEM one calculated with 4 d.o.f. if the

TABLE 4
Fundamental linear frequency parameter $\lambda = \omega_\ell^2 mL^4/EI$, *ss beam*

Exact [28]	FEM [31] (eight elements-32 d.o.f.)	FEM [8] (six elements-12 d.o.f.)	HFEM (1 element-4 d.o.f.*)
97·409	97·409	97·419	97·409

*six d.o.f., if symmetries are not used to reduce the number of d.o.f. m — mass per unit length.

TABLE 5
Comparison of $(\omega/\omega_{\ell 1})$ of *ss beam*: *two harmonics*

w_m/r	$\omega/\omega_{\ell 1}$ Exact [32]	$\omega/\omega_{\ell 1}$ [23] 46 d.o.f.	w_m/r	$\omega/\omega_{\ell 1}$ [8] 24 d.o.f.	w_m/r	$\omega/\omega_{\ell 1}$ HFEM 14 d.o.f. (8 d.o.f.*)	w_m/r	$\omega/\omega_{\ell 1}$ HFEM 16 d.o.f (9 d.o.f.*)
1·0	1·0892	1·0892	1·0087	1·0906	0·0995	1·0891	1·0014	1·0894
2·0	1·3177	1·3178	1·9738	1·3106	2·0021	1·3185	2·0001	1·3180
3·0	1·6256	1·6255	2·9808	1·6198	3·0012	1·6268	3·0033	1·6275

*If symmetries are used to reduce the number of d.o.f. of HFEM model.

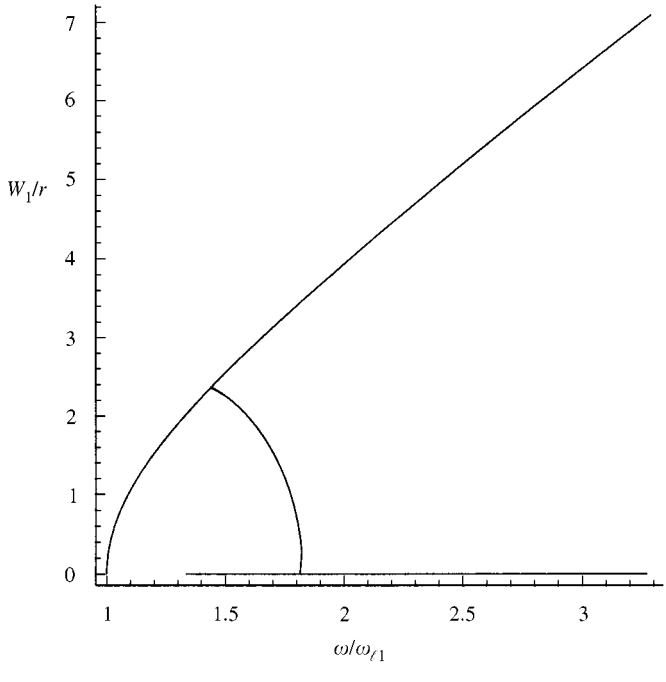

Figure 12. Backbone curve of ss beam defined by W_1/r and $\omega/\omega_{\ell 1}$. From above: first main branch, secondary branch, second main branch.

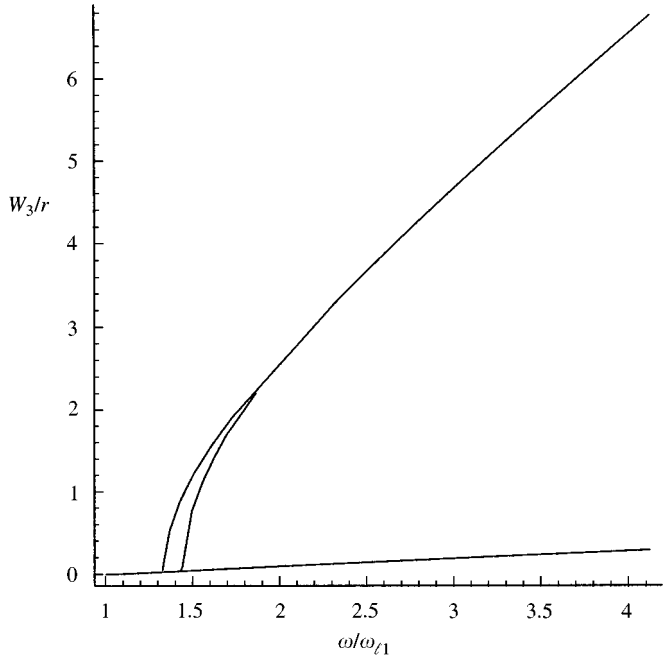

Figure 13. Backbone curve of ss beam defined by W_3/r and $\omega/\omega_{\ell 1}$. From above: second main branch, secondary branch, first main branch.

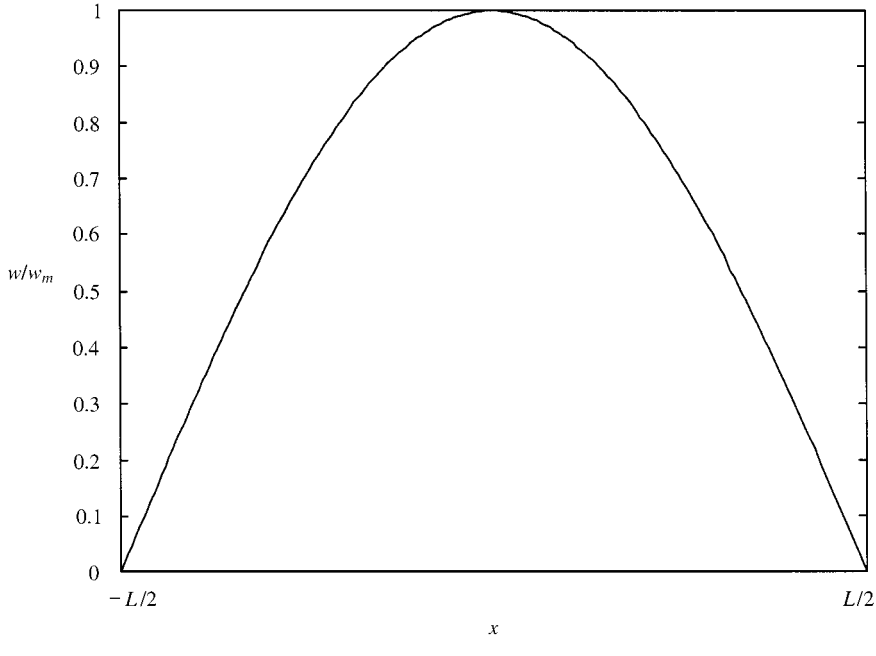

Figure 14. Linear mode shape (—), first (— ·) and third harmonics (..) at $W_1/r \cong 6{\cdot}09$. Difference not visible.

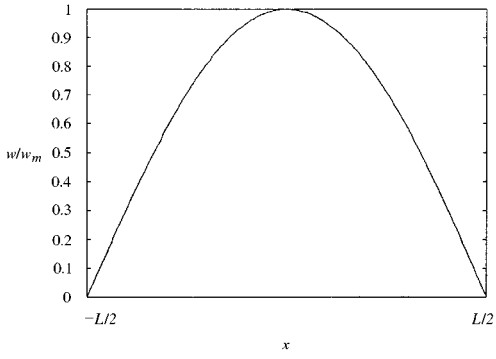

(a) First harmonic of all points of the secondary branch

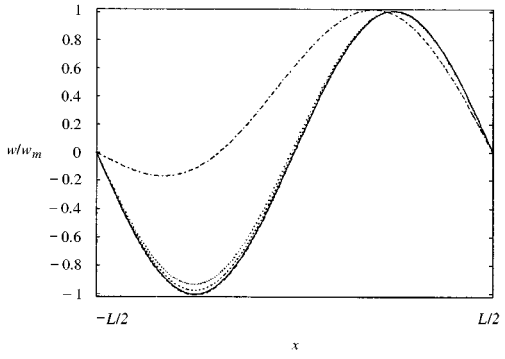

(b) Third harmonic at : – – $\omega/\omega_{\ell 1}$ = 1.303, ...1.352, – – – 1.411, — 1.530, 1.647

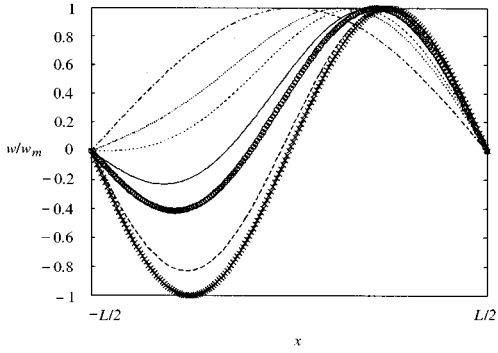

(c) Sum of first and third harmonic at – – $\omega/\omega_{\ell 1}$ = 1.303, ... 1.352, – – 1.411, – 1.530, o 1.589, — — 1.647, + 1.650.

Figure 15. Mode shapes of the secondary branch.

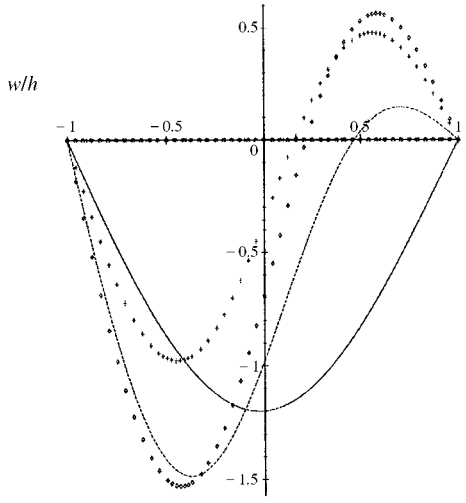

(a) o t = 4T/24, + 5T/24, ◊ 6T/24, – – 7T/24, — 8T/24

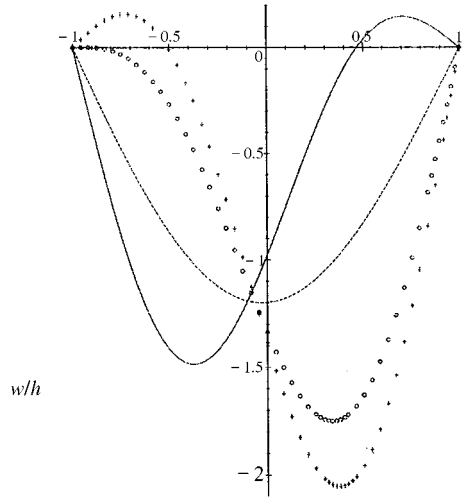

(b) o t=9T/24, + 10T/24, o 11T/24, – – 12T/24, — 13T/24

Figure 16. Vibration of ss beam at $\omega/\omega_{\ell 1} = 1{\cdot}693$, secondary branch.

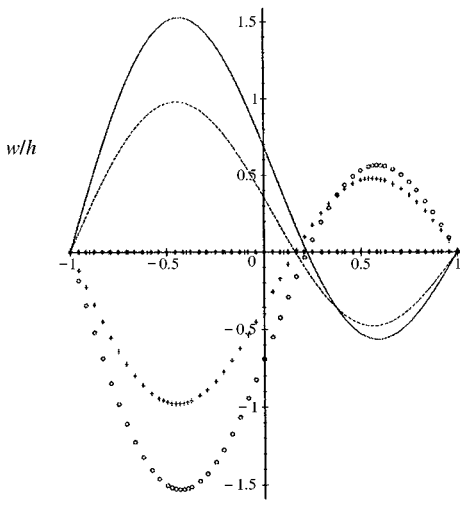

(c) o t=14T/24, + 15T/24, ◊ 16T/24, − − 17T/24, − 18T/24

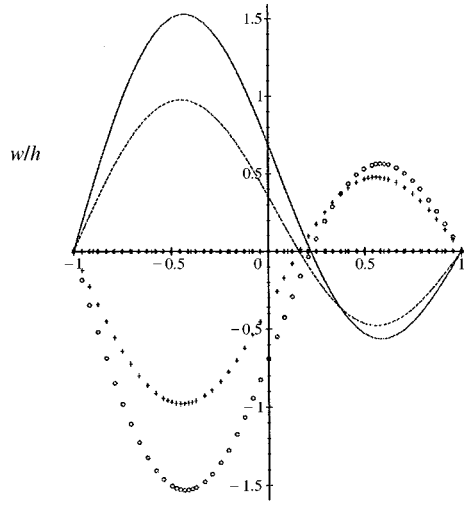

(d) o t = 19T/24, + 20T/24, ◊ 21T/24, − − 22T/24, — 23T/24

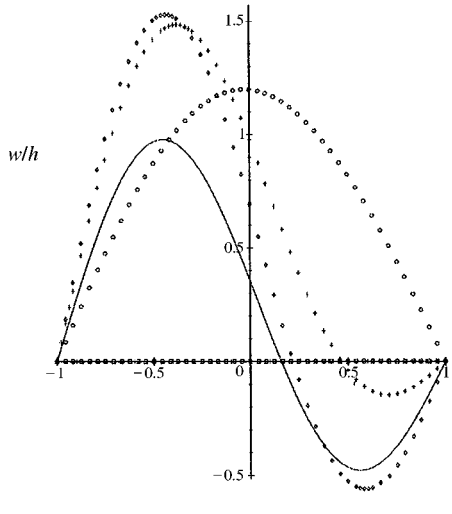

(e) o t = 24T/24, + 25T/24, ◊ 26T/24, − 27T/24, □ 28T/24

Figure 16. Continued

symmetry of the system is used, and with 6 d.o.f. otherwise. In reference [31], 32 d.o.f. were used to obtain the same result as with 4 (6) d.o.f. with the HFEM. In Table 5, the HFEM non-linear resonance frequencies are compared with published ones [8, 23, 32], w_m is the amplitude of vibration displacement at $x = 0$. Again, the HFEM model required fewer d.o.f. than the h-version of the FEM. Results of HFEM models with 14 and 16 d.o.f. are shown in order to demonstrate the convergence of the solution.

Figure 12 shows the backbone curve of a simply supported beam, defined by the non-dimensional amplitude of the first harmonic at the middle of the beam, W_1/r,

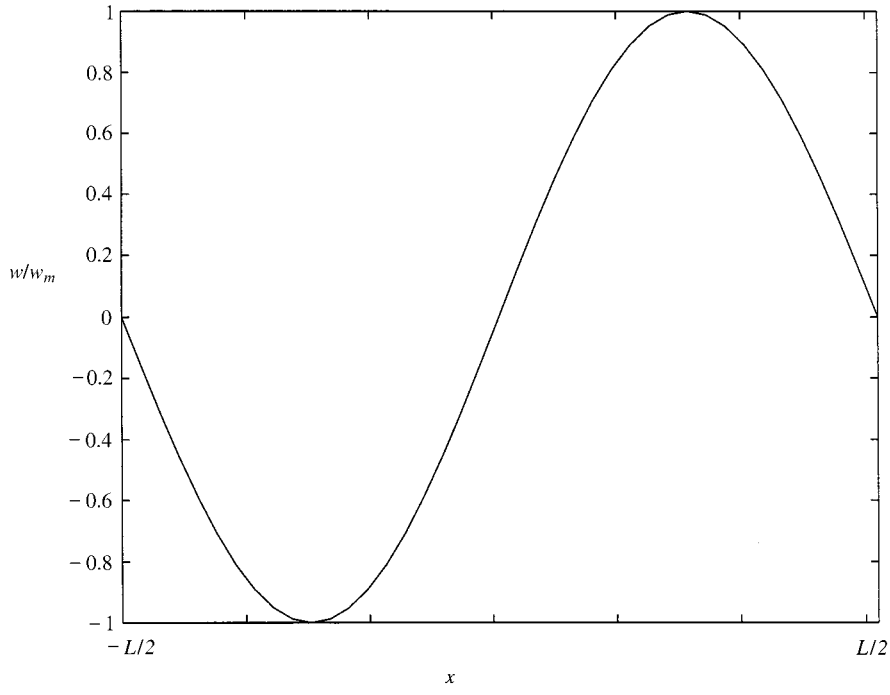

Figure 17. Non-linear mode shapes of the second main branch.

and by the non-dimensional non-linear resonance frequency, $\omega/\omega_{\ell 1}$. There is a main branch, with a shape initially parabolic and tending to rectilinear, that starts at the linear frequency. There was also found to be a secondary branch, which bifurcates from the main branch for a non-dimensional frequency in the range $1{\cdot}439 < \omega/\omega_{\ell 1} < 1{\cdot}442$. The determinant of the matrix [**J**] changed sign between these two successive points.

The first non-linear resonance frequency, $\omega_{n\ell 1}$, around which occurs the first bifurcation point is equal to $\omega_{\ell 2}/2{\cdot}78$, where $\omega_{\ell 2}$ is the second natural linear frequency. As the amplitude of vibration increases, the second non-linear natural frequency also increased ($\omega_{n\ell 2} > \omega_{n\ell 2}$). Then, at a point for which $1{\cdot}439 < \omega/\omega_{\ell 1} < 1{\cdot}442$, the first non-linear resonance frequency is nearly equal to one-third of the second non-linear resonance frequency, $\omega_{n\ell 1} \cong \omega_{n\ell 2}/3$, and an internal resonance exists: there is a strong coupling and a transfer of energy between the first and the second mode. This internal resonance results in a bifurcation point, which is very close to the one found in reference [8] at $1.446 < \omega/\omega_{\ell 1} < 1.451$.

Finally, there is another branch, which begins at $\omega/\omega_{\ell 1} = 1{\cdot}333$ and crosses the secondary branch at $\omega/\omega_{\ell 1} \cong 1{\cdot}82$. This branch was found in reference [33], using an analytical method which gives a qualitative information.

In Figure 13, the backbone curve defined by W_3/r and $\omega/\omega_{\ell 1}$ is presented. W_3 is the amplitude of the third harmonic calculated at $x = 0{\cdot}25 \times L$ (near the point of maximum amplitude of the second mode shape). This figure shows that, in the main

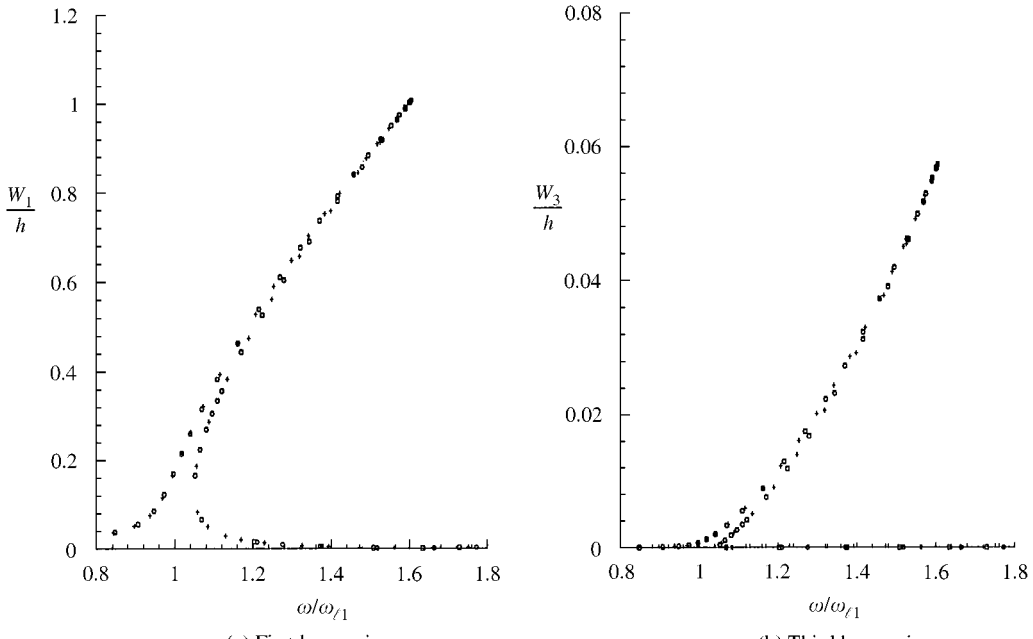

(a) First harmonic (b) Third harmonic

Figure 18. FRF near first resonance frequency of cc beam calculated with: ○ $p_o = 5$, + $p_o = 7$, □ $p_o = 9$, at point $x = 0{\cdot}25 \times L$. In all cases $p_i = 10$.

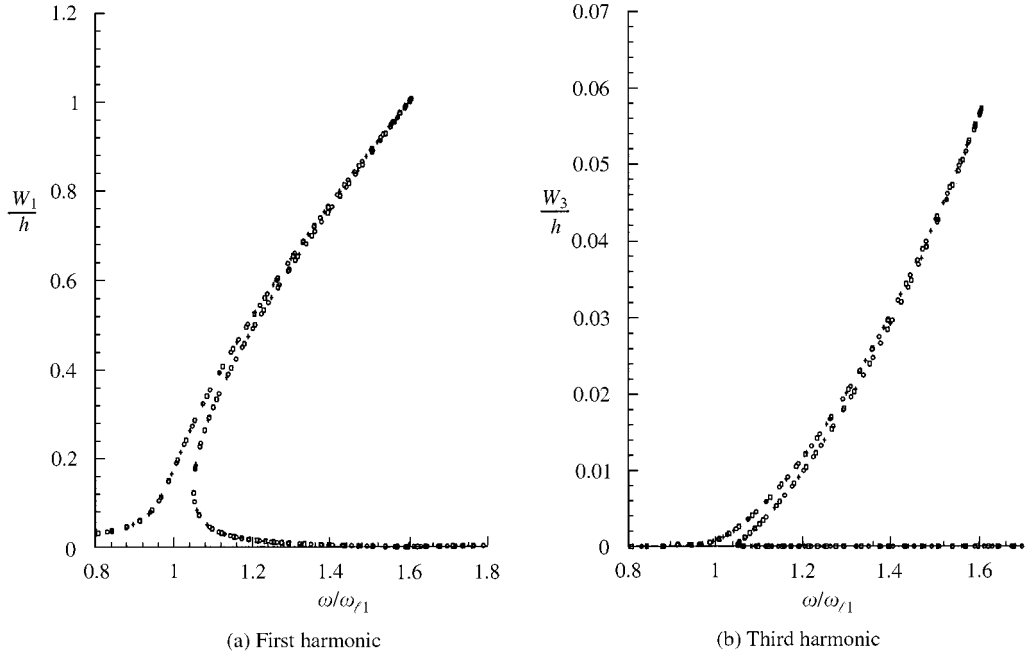

(a) First harmonic (b) Third harmonic

Figure 19. FRF near first resonance frequency of cc beam calculated with: ○ $p_i = 8$, + $p_i = 10$, □ $p_i = 12$, at point $x = 0{\cdot}25 \times L$. In all cases $p_o = 7$.

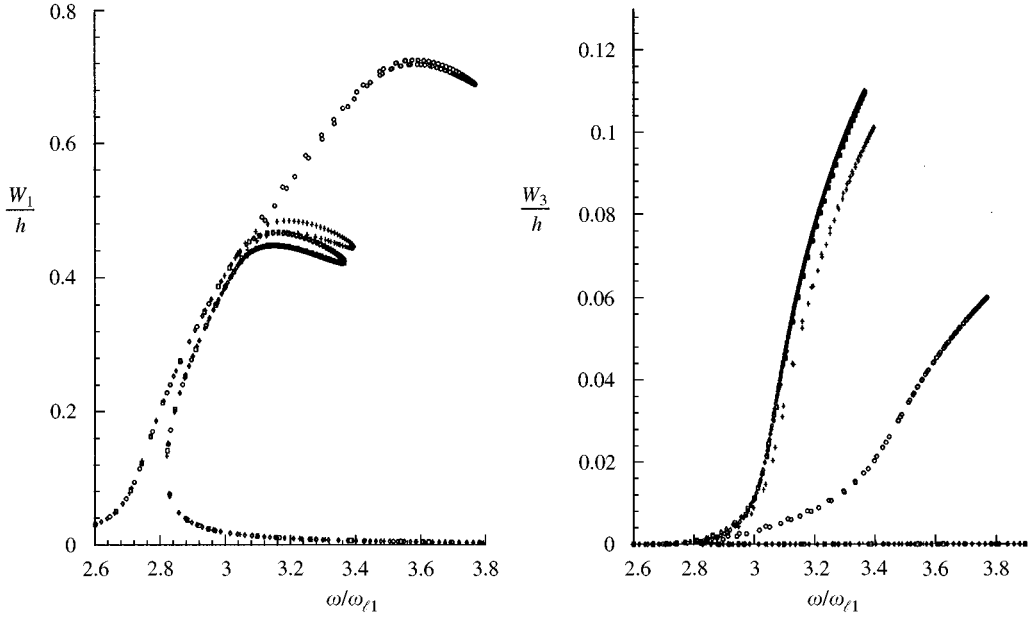

(a) First harmonic (b) Third harmonic

Figure 20. FRF near first resonance frequency of cc beam calculated with $p_i = 10$ and: ○ $p_o = 5$, + $p_o = 7$, □ $p_o = 9$, ◇ $p_o = 11$ ($x = 0{\cdot}25 \times L$).

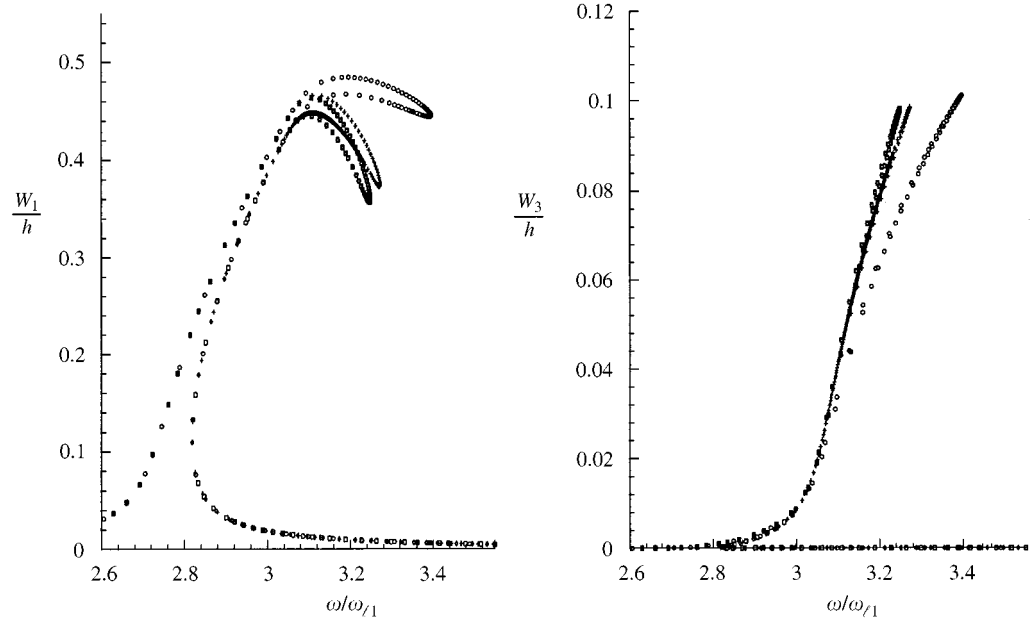

(a) First harmonic (b) Third harmonic

Figure 21. FRF near second resonance frequency of cc beam calculated with $p_o = 7$ and: ○ $p_i = 10$, + $p_i = 12$, □ $p_i = 14$, ◇ $p_i = 16$ ($x = 0{\cdot}25 \times L$).

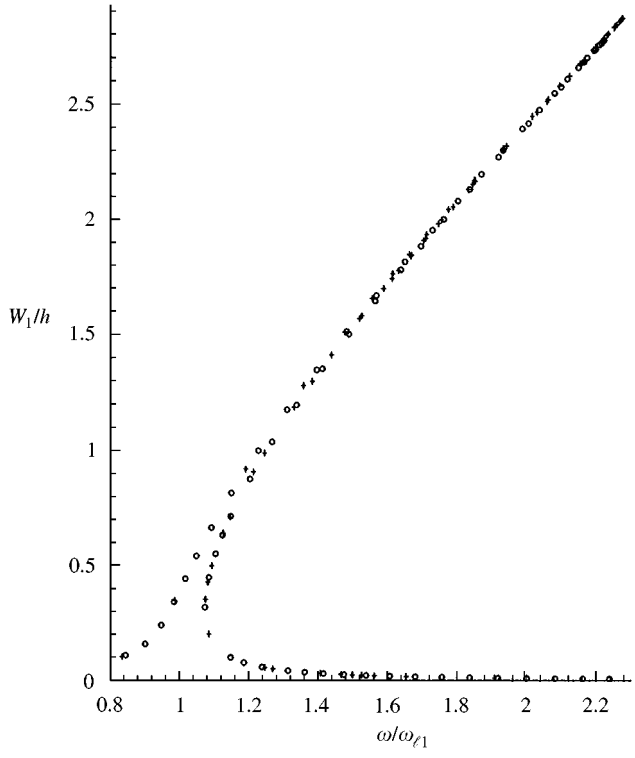

Figure 22. Amplitude of first harmonic (at $x = 0$) due to point harmonic excitation of 0.03 N amplitude, applied in the middle of cc beam: + harmonic solution, ○ two-harmonics solution: $\alpha = 0{\cdot}01$, $p_o = 7$, $p_i = 10$.

branch, the third harmonic has a very small influence on the vibration characteristics of the beam. However, the third harmonic has a significant weight the secondary branch and the second main branch, is almost only defined by the third harmonic.

In the first main branch, the non-linear modes associated with the first harmonic and the third harmonic (almost zero in this branch) are identical to the first linear mode shape (Figure 14), agreeing with reference [3].

Figures 15(a–c) display some non-linear mode shapes associated with points of the secondary branch. The first harmonic has always a shape similar to the first mode shape of a simply supported beam. The third harmonic has a shape that is mainly a mixture of the first and second modes, but, as one proceeds along the branch, it quickly approaches the second mode shape of a simply supported beam. Also, proceeding from the bifurcation point, the weight of each harmonic in the definition of the complete mode shape of vibration changes: the first harmonic gradually vanishes and the third harmonic gradually increases [Figures 12, 13 and 15(c)]. Thus, in the secondary branch, the resultant shape of the deflected beam is asymmetrical, starting from a symmetrical mode shape at the first branch point and finishing in an antisymmetrical mode shape at the second bifurcation point. As in Figure 6, Figure 15(c) was computed at $t = 2\pi mT$, with m an integer.

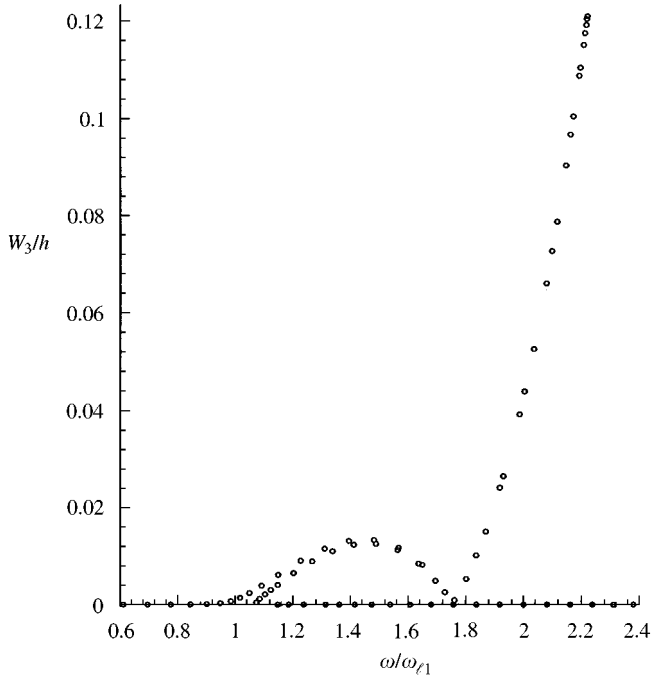

Figure 23. Amplitude (at $x = 0$) of third harmonic due to point harmonic excitation of 0.03 N amplitude, applied in the middle of cc beam. $\alpha = 0{\cdot}01$, $p_o = 7$, $p_i = 10$.

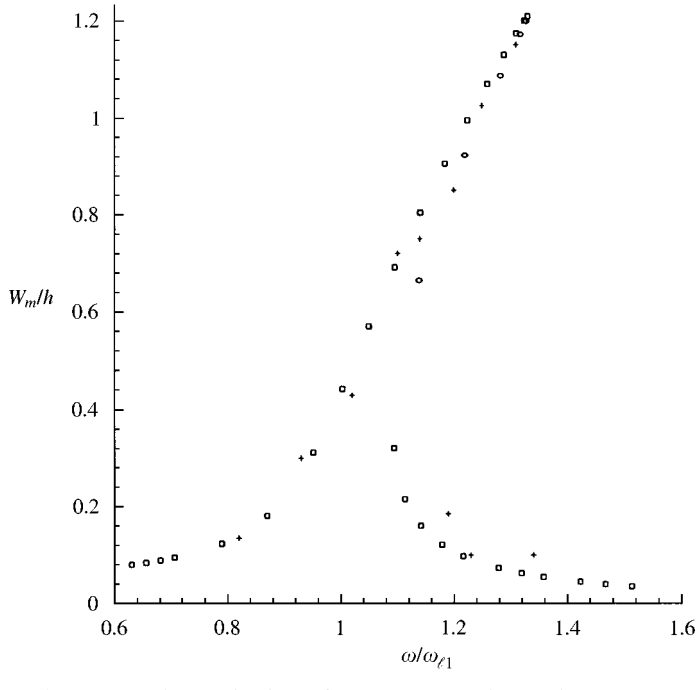

Figure 24. FRF due to a point excitation of 0·134 N: experimental +, HFEM ($p_o = 6$, $p_i = 8$, $\alpha = 0{\cdot}038$) □ stable, ○ unstable. Values at point $x = 0$.

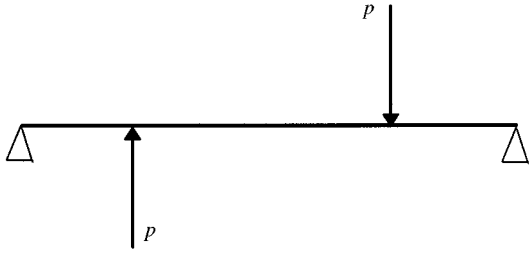

Figure 25. Antisymmetric excitation.

Figure 16 shows the variation of the mode shape of the beam during a half of the period of vibration and for a particular frequency of vibration. This variation is only meaningful in the secondary branch, where both harmonics are important.

In Figure 17, the non-linear mode shape associated with the second main branch is displayed. This non-linear mode is defined solely by the third harmonic and is the same for any amplitude of vibration displacement. It is equal to the first antisymmetric or second mode shape of a hinged–hinged beam: hence it starts at 113·367 rad/s ($113{\cdot}367 \times 3 = 340{\cdot}1$, which is the second linear normal frequency).

4.3. STEADY-STATE FORCED VIBRATION

4.3.1. Clamped–clamped beam

In order to study the consequences of 1 : 3 internal resonances in the steady-state forced vibration of the clamped–clamped beam, a model with two harmonics, the first and the third was used. As was verified in Section 4.2.1, two harmonics are enough to study 1 : 3 internal resonances. Damping was calculated by expression (37), with $\alpha = 0{\cdot}01$.

Figures 18–20 show the variation of the amplitudes of the first, W_1, and third, W_3, harmonics of the cc beam as functions of the frequency of excitation. These amplitudes are given by

$$W_1 = \sqrt{w_{c1}^2 + w_{s1}^2}, \tag{51}$$

$$W_3 = \sqrt{w_{c3}^2 + w_{s3}^2}, \tag{52}$$

where w_{c1}, w_{s1}, w_{e3} and w_{c3} are, in this order, the amplitudes of the cosine and sine terms of the first and third harmonics. Thus, W_1 and W_3 are always positive. In order to excite symmetric and antisymmetric modes, an asymmetric excitation was applied. This was a point harmonic force at $x = L/4$; the response is calculated also at this point.

Around the first mode, both harmonics are well approximated with five out-of-plane and eight in-plane shape functions (Figures 18 and 19).

Around the second resonance frequency and at the largest amplitudes of vibration displacement, the FRF curve of the first harmonic has a very different shape from the usual curve derived in harmonic vibration. The fourth linear natural

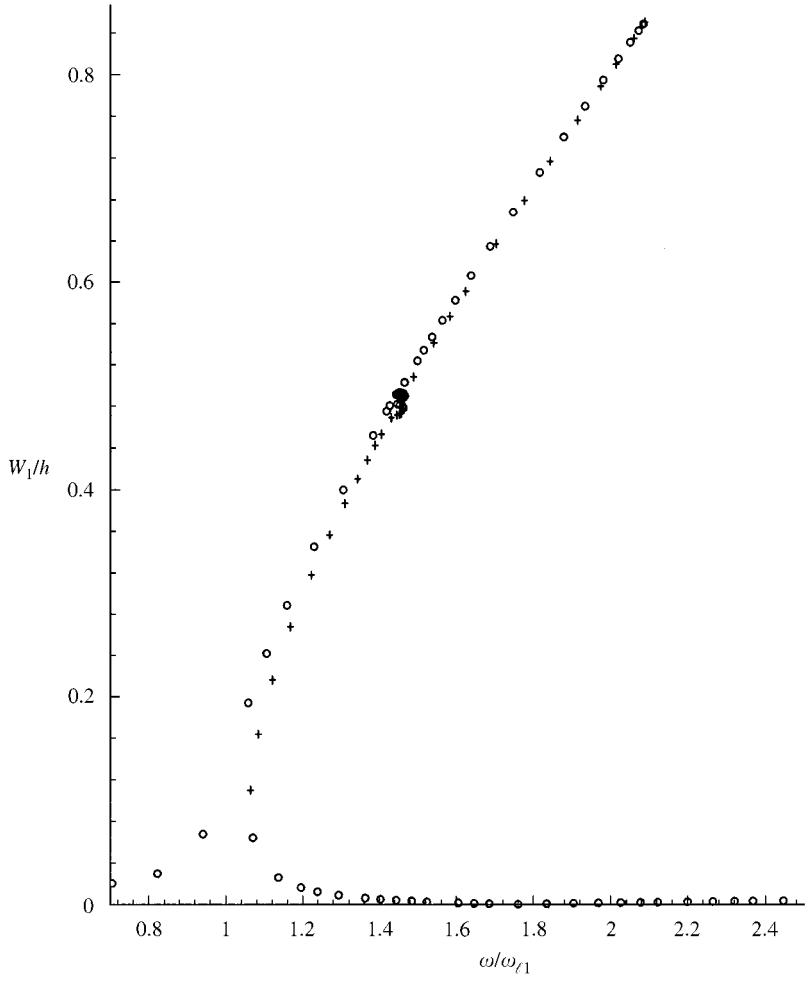

Figure 26. Amplitude of first harmonic (at $x = L/4$) due to antisymmetric excitation: + unstable solution, ○ stable solution. $\alpha = 0{\cdot}01$, $p_o = 10$, $p_i = 10$.

frequency, $\omega_{\ell 4}$, is approximately equal to $3{\cdot}24\omega_{\ell 2}$ (Table 1). Therefore, when $\omega_{n\ell 2}$ increases, there is a point when $\omega_{n\ell 4}/\omega_{\ell 2} \cong 3$ and the fourth mode is excited due to a 1:3 internal resonance between the second and fourth modes. Consequently, at least seven out-of-plane shape functions (nine, if very good accuracy is required) and 14 in-plane shape functions are necessary to describe the FRF in the vicinity of the second resonance frequency (Figures 20 and 21).

In the absence of internal resonance, five out-of-plane shape functions (three symmetric and two antisymmetric), i.e. 20 d.o.f., give good results for the first two modes. If internal resonance occurs, then more d.o.f. are necessary to study the first two mode (28 or 36 d.o.f., depending on the accuracy desired).

In Figures 22 and 23, the frequency response curves due to a point force of amplitude $P = 0{\cdot}03$ N, applied the middle of the beam are shown. The maximum amplitude of the first harmonic is smaller when calculated with two harmonics than when calculated with one harmonic. The third harmonic amplitude increases

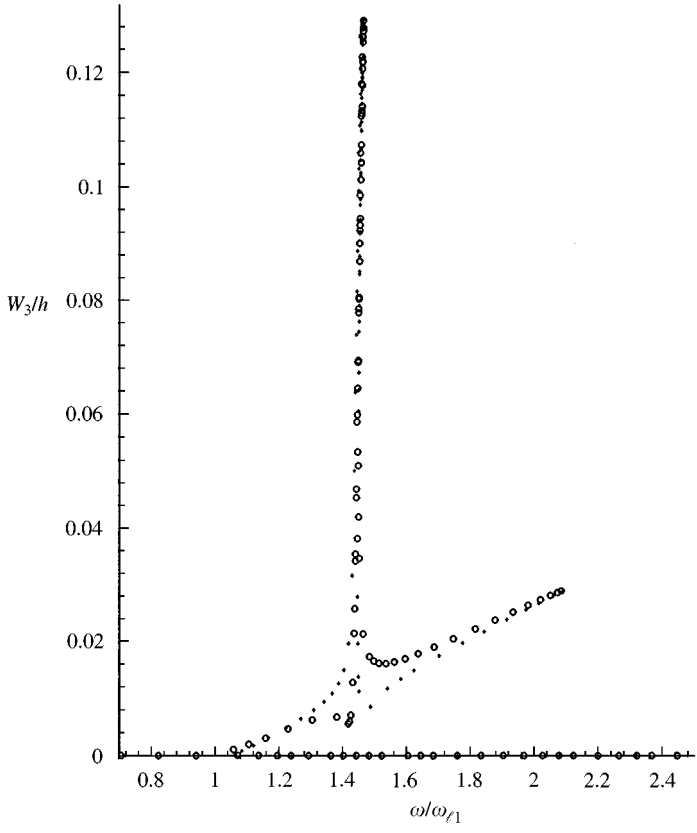

Figure 27. Amplitude of third harmonic (at $x = L/4$) due to antisymmetric excitation: + unstable solution, ○ stable solution. $\alpha = 0{\cdot}01$, $p_o = 10$, $p_i = 10$.

significantly after $\omega/\omega_{n\ell 1} > 1{\cdot}8$. At this point, $\omega_{n\ell 3}/\omega_{n\ell 1} = 3$ and the third mode is excited. Thus, some of the energy that in the one harmonic solution is absorbed between the first mode, in the two harmonics solution is divided by the first and third modes.

In Figure 24, the HFEM solutions are compared with experimental results [34] and the agreement is excellent. Due to the absence of internal resonances, a one harmonic approach gives very accurate results.

4.3.2. *Simply supported beam*

In order to clearly demonstrate the existence of a 1 : 3 internal resonance between the first and second modes, the simple supported beam was excited with an antisymmetric force system, as shown in Figure 25 with $P = 0{\cdot}008$ N. Figure 26 show the consequences of a 1 : 3 internal resonance: a loop in the ascending part of the FRF curve and another loop in the descending part of the FRF curve. The results obtained agree with the ones published in references [9, 10]. Figure 27 shows that these loops are associated with a strong local excitation of the third harmonic. The first-order stability of the solutions was analyzed by using the sign of $|\mathbf{J}|$ [9, 10].

5. CONCLUSIONS

Geometrically non-linear multi-harmonic free and steady-state forced vibrations of cc and ss isotropic beams were studied by the hierarchical finite-element method.

1 : 3 and 1 : 5 internal resonances were found in free vibration. They result in an accentuated change of the curvature of the backbone curve or in secondary branches. 1 : 3 internal resonances were discovered in forced vibration and resulted in loops of the frequency response function curves.

Internal resonances of order n exist if the ratio of the linear frequencies associated with the interacting modes of vibration is approximately equal to n ($\omega_{\ell k2}/\omega_{\ell k1} \cong n$, where the subscripts $k1$ and $k2$ represent two different modes). When analyzing a certain mode of vibration and when the non-linear frequency becomes a submultiple of another natural frequency, it is necessary to include another harmonic in the time series. Below that point, the solution with only one harmonic produces data that is sufficiently accurate, as was confirmed by comparison with experimental results. The coupling with higher order modes also implies that more d.o.f. are necessary in the spatial model for accuracy.

The non-linear mode shape changes with the amplitude and frequency of vibration because of two different causes. The first, is the variation of the stiffness of the beam with the amplitude of vibration, due to the membrane forces. In this case, the alteration in the non-linear mode shape is moderate. The second cause of alteration is modal coupling. If there is commensurability of natural frequencies and internal resonance occurs, then the non-linear vibration of the beam is defined by the sum of the coupled modes vibrating at commensurable frequencies, and the mode shape varies significantly during the period of vibration.

The HFEM model was favourably compared with FEM models presented in the literature. With the HFEM, convergence was achieved with fewer d.o.f. which significantly reduces the computational time. This turns out to be of great importance if one wants to analyze higher order modes or when higher order modes couple with lower order modes due to internal resonance, if several harmonics must be included in the time series or if a structure composed of several beams is to be studied.

ACKNOWLEDGMENT

P. Ribeiro gratefully acknowledges the scholarship PRAXIS XXI/BD/3868/94 from the *Fundação para a Ciência e a Tecnologia*, Portugal.

REFERENCES

1. R. M. Rosenberg 1996 *Advances in Applied Mechanics* **9**, 155–242. On non-linear vibrations of systems with many degrees of freedom.
2. M. M. Bennouna and R. G. White 1984 *Journal of Sound and Vibration* **96**, 309–331. The effects of large vibration amplitudes on the fundamental mode shape of a clamped–clamped uniform beam.
3. R. Benamar, M. M. Bennouna and R. G. White 1991 *Journal of Sound and Vibration* **149**, 179–195. The effects of large vibration amplitudes on the mode shapes and natural frequencies of thin elastic structures. Part I: simply supported and clamped–clamped beams.

4. W. Szemplinska-Stupnicka 1990 *The Behaviour of Non-linear Vibrating Systems*. Dordrecht: Kluwer Academic Publishers.
5. A. H. Nayfeh and D. T. Mook 1995 *Nonlinear Oscillations*. New York: Wiley
6. A. H. Nayfeh and B. Balachandran 1989 *Applied Mechanics Review* **42** S175-S201. Modal interactions in dynamical and structural systems.
7. A. Y. T. Leung and T. C. Fung 1989 *International Journal for Numerical Methods in Engineering* **28**, 1599–1618. Non-linear steady state vibration of frames by finite element method.
8. R. Lewandowski 1994 *Journal of Sound and Vibration* **170**, 577–593. Non-linear free vibrations of beams by the finite element and continuation methods.
9. R. Lewandowski 1997 *International Journal Solids Structures* **34**, 1925–1947. Computational formulation for periodic vibration of geometrically nonlinear structures — Part 1: theoretical background.
10. R. Lewandowski 1997 *International Journal Solids Structures* **34,** 1949–1964. Computational formulation for periodic vibration of geometrically nonlinear structures — Part 2: numerical strategy and examples.
11 L. Meirovitch and H. Baruh 1983 *International Journal for Numerical Methods in Engineering* **19,** 281–291. On the inclusion principle for the hierarchical finite element method.
12. N. S. Bardell 1991 *Journal of Sound and Vibration* **151**, 263–289. Free vibration analysis of a flat plate using the hierarchical finite element method.
13. W. Han 1993 *Ph.D. Thesis, University of Southampton*. The analysis of isotropic and laminated rectangular plates including geometrical non-linearity using the *p*-version finite element method.
14. W. Han and M. Petyt 1997 *Computers and Structures* **63,** 295–308. Geometrically nonlinear vibration analysis of thin, rectangular plates using the hierarchical finite element method — I: the fundamental mode of isotropic plates.
15. W. Han and M. Petyt 1997 *Computers and Structures* **63**, 309–318. Geometrically nonlinear vibration analysis of thin, rectangular plates using the hierarchical finite element method — II: 1st mode of laminated plates and higher modes of isotropic and laminated plates.
16. A. Houmat 1997 *Journal of Sound and Vibration* **201**, 465–472. Hierarchical finite element analysis of the vibration of membranes.
17. A. Houmat 1997 *Journal of Sound and Vibration* **206**, 201–215. An alternative hierarchical finite element formulation applied to plate vibrations.
18. P. Ribeiro and M. Petyt 1999 *International Journal of Mechanical Sciences* **41**, 437–459. Nonlinear vibration of plates by the hierarchical finite element and continuation methods.
19. B. A. Szabó and I. Babuska 1991 *Finite Element Analysis*. New York: Wiley.
20. C. Y. Chia 1980 *Nonlinear Analysis of Plates*. New York: McGraw-Hill.
21. O. C. Zienkiewicz and R. L. Taylor 1988 *The Finite Element Method*. London: McGraw-Hill, fourth edition.
22. M. Petyt 1990 *Introduction to Finite Element Vibration Analysis*. Cambridge: Cambridge University Press.
23. Y. K. Cheung and S. L. Lau 1982 *Earthquake Engineering and Structural Dynamics* **10,** 239–253. Incremental time-space finite strip method for non-linear structural vibrations.
24. T. J. Mentel 1959 *Colloquium on Structural Damping*, (J. E. Ruzicka, editor, 89–116. New York: The American Society of Mechanical Engineers. Vibrational energy dissipation at structural support junctions.
25. D. Redfern 1994 *The Maple Handbook*. New York: Springer-Verlag.
26. C. K. Chiang, C. Mei and C. E. Gray 1991 *Transactions of the ASME, Journal of Vibration and Acoustics* **113**, 309–315. Finite element large-amplitude free and forced vibrations of rectangular thin composite plates.

27. P. Ribeiro and M. Petyt 1995 *Institute of Sound and Vibration Research Tech. Mem. No. 773*. Study of nonlinear free vibration of beams by the hierarchical finite element method.
28. C. M. Harris 1988 *Shock and Vibration Handbook*. New York: McGraw-Hill, third edition.
29. M. M. K. Bennouna 1982 *Ph.D. Thesis, University of Southampton*. Nonlinear dynamic behaviour of a clamped-clamped beam with consideration of fatigue life.
30. R. Benamar 1990 *Ph.D. Thesis, University of Southampton*. Nonlinear dynamic behaviour of fully clamped beams and rectangular isotropic and laminated plates.
31. B. S. Sarma and T. K. Varadan 1984 *International Journal for Numerical Methods in Engineering* **20**, 353–367. Ritz finite element approach to non-linear vibrations of beams.
32. S. Woinowski-Krieger 1950 *Journal of Applied Mechanics* **17,** 35–36. The effect of an axial force on the vibration of hinged bars.
33. R. Lewandowski 1994 *Journal of Sound and Vibration* **177,** 239–249. Solutions with bifurcation points for free vibration of beams: an analytical approach.
34 H. Wolfe 1995 *Ph.D. Thesis, University of Southampton*. An experimental investigation of nonlinear behaviour of beams and plates excited to high levels of dynamic response.

APPENDIX

Out-of-plane shape functions:

$$f_1 = (1/8) - (1/8)\xi - (1/8)\xi^2 + (1/8)\xi^3,$$

$$f_2 = -(1/8) - (1/8)\xi + (1/8)\xi^2(1/8)\xi^3.$$

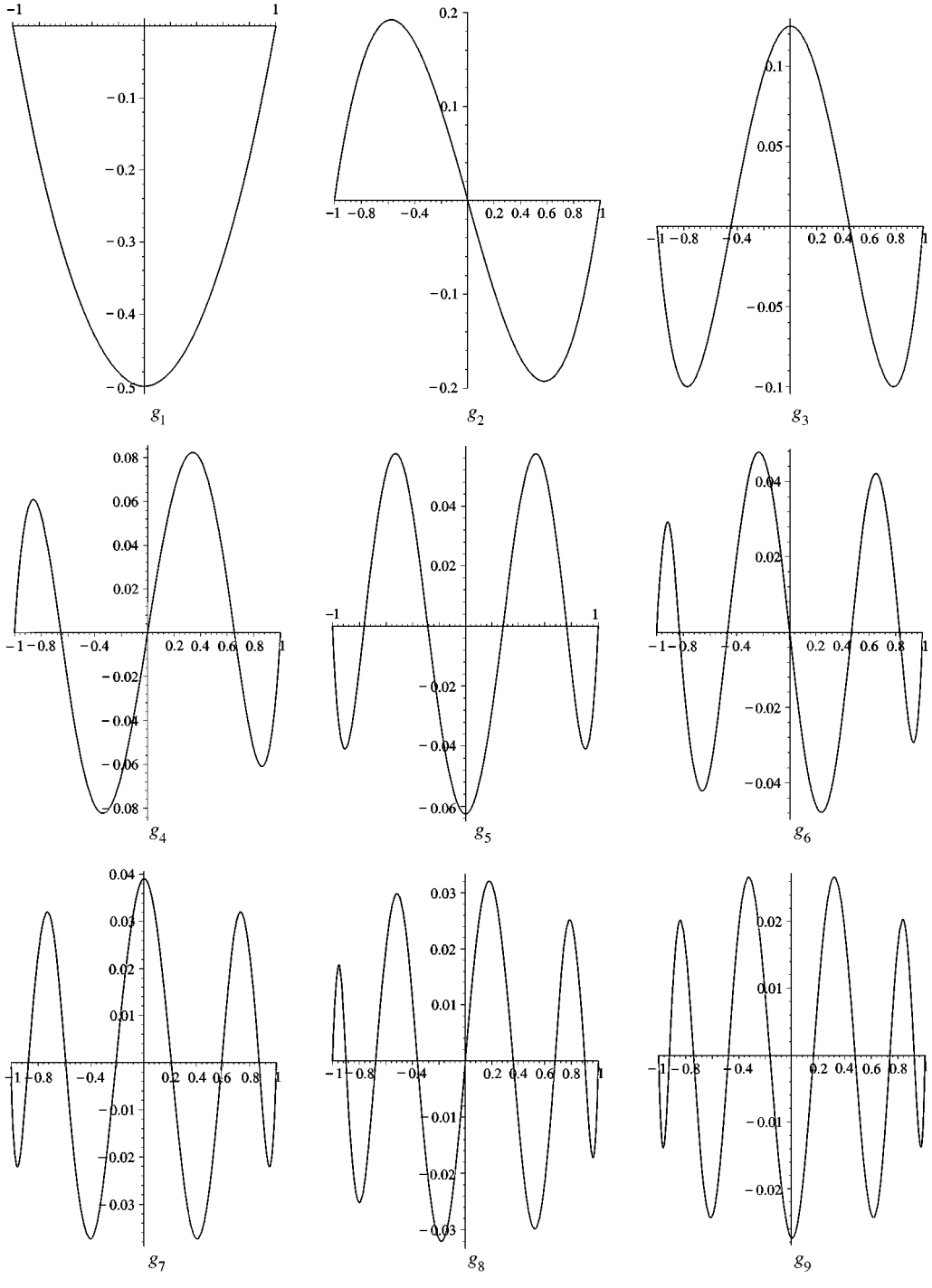

In-plane shape functions: